Satellite data for the integrated modelling of Watershed-Coast System morphodynamics in a changing climate: a critical review and a structured framework

Achilleas G. Samaras[1] and Michael Nones[2]

[1]Department of Civil Engineering, Democritus University of Thrace, University Campus - Kimmeria, 67100 Xanthi, Greece

https://orcid.org/0000-0002-0201-3695

[2]Institute of Geophysics, Polish Academy of Sciences, Ks. Janusza 64, 01-452 Warsaw, Poland

https://orcid.org/0000-0003-4395-2637

Corresponding Author: Achilleas G. Samaras, achsamar@civil.duth.gr, +30 25410 79615.

Statement: The paper is a non-peer reviewed preprint submitted to EarthArXiv. The paper has been submitted for peer review to "Earth Science Reviews" (Elsevier).

Abstract

Watershed-Coast Systems (WACS) integrate the watershed and the coast as a coupled geomorphological entity whose evolution depends on climate, terrestrial, and marine drivers acting at very different scales. Modelling the morphodynamics of WACS in a changing climate is a recognised but uneven endeavour: satellite-data use has matured for inland hydrology and for coastal observation taken in isolation, but the role of satellite data as the connective tissue between the two – the integration component of recent WACS frameworks – remains comparatively underdeveloped. This review addresses that asymmetry. It synthesises the literature on the use of satellite data for each component of an established WACS modelling framework (climate, watershed, coastal, and integration), with particular attention to the river-mouth, estuary, and delta interface where satellite observations bridge terrestrial and marine processes. A structured methodological framework is then proposed that operationalises the use of satellite data within the WACS modelling workflow; the framework is organised and visualised by matrices connecting essential aspects to satellite-product families, to modelling roles, and to spatial and temporal scales. The framework foregrounds the modelling roles (forcing, parameterisation, calibration, assimilation, validation, assessment, communication) and explicitly identifies where current missions are productive and where gaps remain, with the recent wide-swath altimetry mission offering a particularly clear opportunity for transitional-zone modelling. The review is intended for scientists, engineers, and modellers working on integrated watershed–coast modelling, and for coastal and river managers and policymakers concerned with WACS resilience.

Keywords

Watershed-Coast Systems; Geomorphology; Morphodynamics Modelling; Climate Change; Satellite Data; Integrated Modelling; Earth Observation.

1. Introduction

The morphological evolution of a coast is governed in large part by the water and sediment that rivers and natural streams deliver to it; accordingly, the watershed and the coastal area adjacent to its outlet do not evolve independently but as one coupled system. Samaras (2023) formalises this coupling as the Watershed-Coast System (WACS). His work decomposes the integrated problem into four fundamental components, i.e. (A) Climate Change, (B) Watershed Dynamics, (C) Coastal Dynamics, (D) Integration of the Watershed-Coast System, and identifies the integration component, independent of the climate forcing, as the element that defines the essence of the concept.

This holistic reading of the river-to-sea continuum is not confined to a single terminology. The watershed–coast coupling has been approached as the "catchment-coast continuum" through which sediment is traced from source to sink (Salomons, 2005), as the "Catchment-Estuary-Coastal" (CEC) system in the reduced-complexity coupled modelling of inlet-interrupted coastlines (Bamunawala et al., 2020), and as the "Watershed-Coast Continuum" (WCC) in the coupling-oriented review of Malara et al. (2020). It is noted that Malara et al. (2020) reach the imperative of a holistic, continuous monitoring of the coupled system without invoking satellite observation at all – precisely the gap that the present work addresses. The WACS framework of Samaras and Koutitas (2014a, 2014b) and Samaras (2023) is retained throughout this work as the organising scaffold, and no new terminology is introduced; the parallel framings are positioned here, in the Introduction, as related descriptions of the same coupled object.

The stakes of the coupling are sharpened by a changing climate. The drivers that the four components must represent – i.e. the precipitation regime and the erosive forcing of the watershed, the wave climate and the mean and extreme sea level at the coast, and the sediment flux that joins them – are each non-stationary, and their projected change propagates through the coupled system to the deltas, estuaries and beaches on which a large fraction of the world's population and infrastructure is concentrated (Laignel et al., 2023). Accordingly, the modelling of WACS morphodynamics is increasingly required not for a stationary present but for a scenario envelope of future states, and the data that constrain that modelling must be commensurate, in coverage and continuity, with the scales of the coupled system.

Satellite Earth observation is, in principle, the data source best matched to that requirement, since it supplies spatially continuous, repeat measurements of precisely the variables the components need: precipitation, soil moisture, terrestrial water storage, river stage and width, wave height, sea level, shoreline position and nearshore bathymetry. The use of these observations is, however, markedly uneven across the system. The watershed (Component B) and the coast (Component C) are each served by a mature and well-reviewed satellite literature, whereas the watershed–coast coupling – operationally the river-mouth, estuary and delta interface that defines Component (D) – is at once the most geomorphologically dynamic link in the chain, the most under-sampled by in situ networks, and the least addressed by the satellite-modelling literature.

Regarding the integration gap itself, the difficulty is less one of data availability than of structure: satellite data are abundant, but they are typically treated as inputs to a single process (e.g. a climate trend, a watershed runoff model, a shoreline analysis) rather than as the connective tissue that allows the coupled system to be studied as a whole. The recent Surface Water and Ocean Topography (SWOT) mission, which natively observes the continental-waters–estuary–ocean continuum in a single swath (Biancamaria et al., 2016), makes this gap both more visible and more closable, since for the first time a single instrument references the landward and seaward water surfaces of the transitional zone to a common field. It is noted that the process-based morphodynamic modelling of estuaries at the decadal scale (Luan et al., 2017) and the reduced-complexity

coupled modelling of the CEC literature each reach towards this integration from the modelling side; the present work approaches it from the observation side.

The work presented in this paper is, accordingly, a hybrid contribution: a critical review of the use of satellite data across the four components of the WACS framework and the Science–Society–Governance dimension that bridges them, together with a structured methodological framework that operationalises that use as matrices essential aspect, by satellite-product family, by modelling role and by spatial/temporal scale. Particular attention is given to the transitional zone, developed as a stand-alone topic, and to SWOT, retained throughout as the named technological centrepiece of the integration argument. Section 2 restates the WACS framework of Samaras (2023) and fixes the vocabulary used hereafter. Section 3 reviews the satellite observation of the system by component, with the transitional zone of Section 3.4 as the principal original synthesis. Section 4 shifts the lens from what satellites observe to how those observations enter the coupling, calibration and validation of models (Section 4.1) and the assessment and communication of their results (Sections 4.2 and 4.3). Section 5 presents the structured framework and its two matrix views. Section 6 discusses the cross-cutting themes and the research agenda that the framework reveals. Finally, Section 7 presents the conclusions drawn from this work.

2. Background: the WACS modelling framework

The conceptual scaffold adopted in this work is the Watershed-Coast System (WACS) framework of Samaras (2023), restated in this Section to fix the vocabulary that is employed throughout the rest of the paper. A Watershed-Coast System denotes a watershed together with the coastal area adjacent to its outlet, where the sediment delivered by rivers and natural streams governs the evolution of coastal morphology. Within this framework the problem is decomposed into four fundamental components (see Fig. 1): (A) Climate Change, (B) Watershed Dynamics, (C) Coastal Dynamics, and (D) Integration of the Watershed-Coast System. Components (B) and (C), as well as the influence of Component (A) on each of them, have been studied in considerable detail over the years. Component (D), by contrast, has received markedly less attention despite its importance, and it is this component – independent of Component (A) – that defines the essence of the WACS concept.

Regarding the role of each component within the integrated modelling chain, Component (A) translates Representative Concentration Pathways into scenarios of future climate pressures through applications of Global and Regional Climate Models, data analysis, and the study of extremes. In Component (B) the terrestrial weather or climate pressures travel downstream to the watershed outlet through the modelling of surface runoff, erosion, and water and sediment routing, whereas in Component (C) the corresponding marine pressures travel onshore through the modelling of ocean and coastal wave dynamics and hydrodynamics, with the coastal morphodynamic models integrating this information in order to simulate morphology evolution. It is noted that the sediment discharge delivered at the watershed outlet operates as the quantitative link between the watershed and the coastal models, and is therefore the variable through which the two fields are coupled during simulations.

Component (D), the Integration of the Watershed-Coast System, is the most critical component for the simulation of coastal morphodynamics, since it identifies and evaluates the codependent processes that shape the morphodynamic response of the system, studies their evolution in space and time, and adapts the modelling framework to validate the present or past morphodynamic status of the system and to project its future behaviour. Accordingly, Component (D) is articulated in three successive stages – the coupling and calibration of the watershed and coastal models, the validation of the coupled system for present or past states, and its application to future states. The watershed–coast coupling is operationally located at the river-mouth

and estuarine interface, a transitional zone that is developed as a stand-alone topic in Section 3.4 and that, together with the structured framework of Section 5, carries the principal contribution of the present work.

Figure 1 presents the methodological framework proposed by Samaras (2023) for the integrated modelling of Watershed-Coast System morphodynamics for management and engineering purposes. The framework suggests that future modelling approaches should be formed and evaluated against four requirements: i) the inclusion of all four components (A, B,C, D); ii) the consideration, when defining future scenarios, of the projected climate-change-induced changes in management practices and engineering works in both the terrestrial and the coastal field; iii) applicability to the spatial and temporal scales that are suitable for watershed and coastal management and engineering; and iv) adaptability to methods that address the ecological and socio-economic implications of the projected changes and that engage the relevant stakeholders. It is noted that the last requirement, which corresponds to the right-hand part of the flowchart, introduces many of the major modelling challenges, and that the satellite-data perspective developed in the present work is operationalised against this framework in the matrices of Section 5.

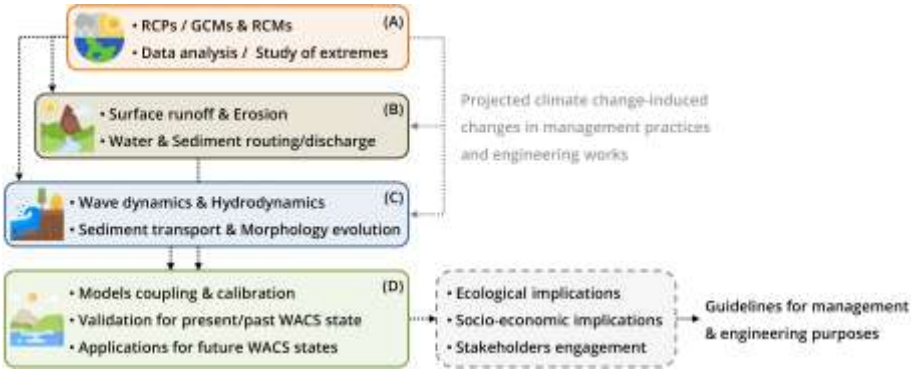


Figure 1. Methodological framework for the integrated modelling of Watershed-Coast System morphodynamics for management and engineering purposes (reused with permission from Samaras, 2023, their Fig. 5).

The translation of modelling advances into resilience is represented in Samaras (2023) by a separate flowchart that bridges the gaps between science, society, and governance, recapitulated here in description only (Fig. 6 of Samaras, 2023). In that flowchart the concepts and the modelling of the system feed the design of protection and adaptation measures and, through a stage of informed decision-making, the translation of strategies into policy and ultimately into the realisation of management practices and engineering works. The region in which science overlaps with society and governance comprises the aspects that are critical for informed decision-making, namely policy analysis, the analysis of the ecological and socio-economic implications of climate-change impacts, the cost-benefit analysis of the proposed measures, and stakeholder engagement. The process is iterative, in that the performance of the measures is assessed after a hazard occurs and that assessment feeds back to the earlier stages, so that resilience is built progressively.

Figure 2 presents the essential aspects through which Samaras (2023) systematises the path towards informed decision-making for the building of resilient Watershed-Coast Systems in a changing climate by means of the integrated modelling of their morphodynamics. These essential aspects (see Table 1) span the drivers of changes in erosion and sediment discharge and in coastal morphology; the role of management practices and engineering works; the association of those drivers with climate-change scenarios and with ecological and socio-economic implications; the seasonality of the pressures and of the codependent processes; the coupling, calibration, and validation of the coupled models (including the decision on the appropriate modelling complexity); and the confrontation of the modelling results for future states with their ecological and socio-

economic implications. These eight aspects provide the row axis of the structured framework operationalised in Section 5, where the coupling, calibration, and validation aspect, being the one most directly tied to Component (D), is examined in a worked walk-through.

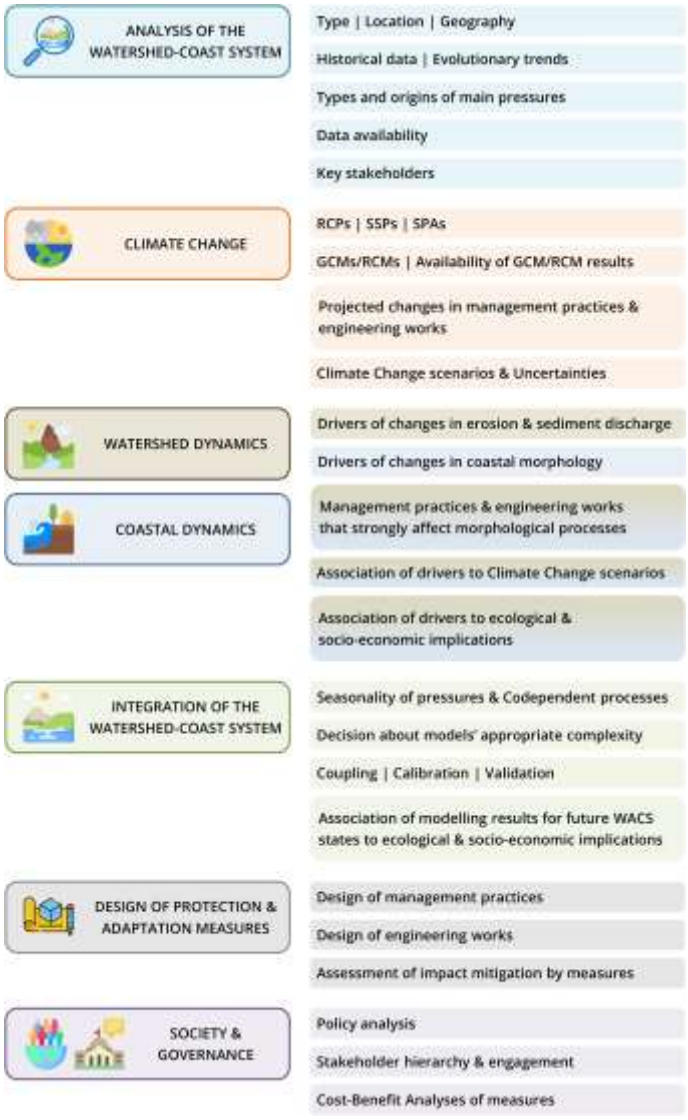


Figure 2. Essential aspects of the path towards informed decision-making for building resilient Watershed-Coast Systems in a changing climate through the integrated modelling of their morphodynamics (reused with permission from Samaras, 2023, their Fig. 7). The eight aspects shown here are defined and mapped to their respective groups based on Samaras (2023) in Table 1.

Table 1. The eight essential aspects (EA1–EA8) of the path to informed decision-making in Samaras (2023), their descriptions, and the group to which each belongs. EA1–EA8 form the row axis of Figures 3–5; this table is therefore the key for reading those matrices and for locating each aspect within the components shown in Figure 2.

Essential Aspect	Description	Group
EA1	Drivers of changes in erosion and sediment discharge	Watershed Dynamics
EA2	Drivers of changes in coastal morphology	Coastal Dynamics
EA3	Management practices and engineering works	Watershed Dynamics, Coastal Dynamics, Design of Measures
EA4	Association of drivers with climate-change scenarios	Climate Change, Watershed Dynamics, Coastal Dynamics
EA5	Association of drivers with ecological and socio-economic implications	Integration of the WACS, Society & Governance
EA6	Seasonality of pressures and codependent processes	Integration of the WACS
EA7	Coupling, calibration and validation of the coupled models (incl. the appropriate-complexity decision)	Integration of the WACS
EA8	Modelling results for future states versus their ecological and socio-economic implications	Design of Measures, Society & Governance

3. Satellite data for the dynamics of the WACS: By-component analysis

3.1. Climate change (Component A)

The role examined in this subsection is the contribution of satellite data to the representation of Climate Change (Component A) within the integrated Watershed-Coast System modelling chain of Samaras (2023). Component (A) supplies the upstream forcing and the scenario envelope against which the watershed, the coast and their coupling are simulated; accordingly, the variables of interest are precipitation intensity, frequency and extremes, land-surface temperature, terrestrial water and mass storage, and surface soil moisture, each of which dictates the drivers of changes in erosion and sediment discharge (essential aspect EA1, see Fig. 2 and Table 1), and the association of those drivers with climate-change scenarios (EA4). The representative product families that observe these variables are satellite precipitation estimates such as the Tropical Rainfall Measuring Mission Multisatellite Precipitation Analysis (TMPA) and the Global Precipitation Measurement Integrated Multisatellite Retrievals (GPM IMERG); optical thermal records from MODIS, Landsat and AVHRR; the gravimetric record of the Gravity Recovery and Climate Experiment (GRACE) and its Follow-On mission; and surface soil moisture of the SMOS/SMAP class. The placement of each within the methodological framework of Fig. 1 is summarised in the matrices of Section 5.

Regarding the forcing role, Huffman et al. (2007) present TMPA as a calibration-based sequential combination of multi-satellite microwave and infrared estimates with gauge analyses at ~0.25° and 3-hourly resolution over the 50°N–S band, providing a fine-scale precipitation field suitable for driving watershed hydrology. A practical motivation for such forcings is that gridded satellite climate fields can substitute for sparse weather-station networks in data-poor basins, a substitution developed for Component (B) in Section 3.2 (Mendelsohn et al., 2007). Building on the TMPA record, Fu and Wu (2024) combine it with GPM IMERG to detect trends in tropical rainfall over 1998–2019, reporting a ~9% decrease in heavy-rain intensity alongside a ~23% increase in light-rain intensity, with heavy-rain frequency rising by ~13% and light-rain frequency falling by ~24%; that is, a

redistribution of rainfall character that propagates directly into the erosive forcing of the watershed. The latter capability extends to extremes, for which Xiao et al. (2020) evaluate seven satellite precipitation products over the Yangtze River Basin for 2003–2017 and find the agreement with gauge reference data to be overall satisfactory, with CMORPH and GPM IMERG capturing extreme-event characteristics relatively well, although most products perform poorly in the mountainous upper reach and in the estuaries of the lower reach.

Satellite observations also calibrate and validate the climate models that generate WACS forcing. Reiners et al. (2023) review satellite-derived land-surface-temperature dynamics across 164 studies and report that MODIS and Landsat records support climate-model evaluation well, while noting that climate-change applications remain underrepresented and that the MODIS-era series is still short for robust trend work. Regarding mass change, Tapley et al. (2019) review the contributions of GRACE to climate science and show that the gravimetric record validates the terrestrial water cycle, ice-mass balance and sea-level budgets and has matured into a reliable mass-transport product underpinning operational drought monitoring; the GRACE signal thereby bridges climate change (Component A) and the watershed storage treated in Section 3.2. The assimilation of these observations into land-surface and catchment models is the more demanding use. Li et al. (2019) assimilate a mascon-based GRACE terrestrial-water-storage product into the Catchment land-surface model at the global scale and point out that, evaluated against nearly 4,000 wells, it reduces groundwater estimation errors by ~36% and ~10% at the regional and point scales; Zaitchik et al. (2008) assimilate GRACE storage anomalies into the same model across four sub-basins of the Mississippi and increase the correlation between simulated storage and gauged river flow in seven of eight smaller watersheds, a route to downscale the coarse GRACE footprint; and Chen et al. (2011) assimilate surface soil moisture of the SMOS/SMAP class into the SWAT catchment model by an ensemble Kalman filter. These assimilation strategies, which couple observations to the model state during the run (essential aspect EA7), are revisited in Section 4.1.

A fourth, downstream use is the assessment of climate-conditioned suspended-sediment and water-quality signals. Jamali et al. (2025) combine satellite image interpretation with QUAL2Kw modelling to track suspended- and dissolved-solids change in the Kichik Chai River (Iran) and to test compliance against water-quality standards. Yan et al. (2025) retrieve river turbidity from forty years of Landsat imagery across Chinese rivers, reporting a mean validation error of ~19 NTU and resolving a four-decade pattern in which western rivers grew more turbid under warming and humidification and eastern rivers cleared under dam construction and management. It is noted that turbidity is treated here as a proxy for suspended particulate matter, which links these studies to the drivers of erosion and sediment discharge (EA1); their river-mouth and downstream signals are taken up again in the transitional zone of Section 3.4.

Nevertheless, several limitations specific to Climate Change (Component A) qualify these uses. Satellite precipitation carries a rate-dependent low bias and limited skill for moderate and light events on short intervals (Huffman et al., 2007), and its accuracy degrades in complex terrain and at river mouths (Xiao et al., 2020), so that the choice of product is itself a sensitivity; the global benchmark of Beck et al. (2017) makes this plain, since, across 22 datasets evaluated against ~76,000 gauges and through hydrological calibration over ~9,000 catchments, the merged satellite–reanalysis–gauge product MSWEP ranked highest, well ahead of single-source estimates. The gravimetric record is coarse in space and monthly in time, requiring assimilation to be useful at catchment scale, and GRACE assimilation does not compensate for processes absent from the host model, such as intensive groundwater abstraction (Li et al., 2019); likewise, weak vertical coupling in the host model limits the depth to which surface soil moisture can constrain the soil column (Chen et al., 2011). All in all, satellite data for Climate Change (Component A) act as forcing, as calibration and validation references, as assimilated state variables, and as assessment proxies. Their structured placement by product family,

modelling role and essential aspect – notably EA1, EA4 and the coupling, calibration and validation aspect EA7 – is operationalised in the matrices of Section 5, where the propagation of the climate signal into the watershed dynamics of Section 3.2, the coastal dynamics of Section 3.3, and the watershed–coast coupling of Section 3.4 is made explicit.

3.2. Watershed Dynamics (Component B)

The Watershed Dynamics (Component B) examined in this work comprise the terrestrial processes that generate and route the water, sediment and associated fluxes ultimately delivered to the coast. The satellite observation of those dynamics is organised here around five coupled sub-domains: weather forcing, relief and soil, land cover and use, inland hydro-morphology and water storage, and the generation of sediment by erosion. Within the integrated framework of Fig. 1, Component (B) supplies the upstream forcing and boundary information on which the downstream coastal and transitional behaviour depends, so that the essential aspects summarised in Fig. 2 and Table 1 (i.e. system forcing, channel and floodplain morphology, sediment supply, land-surface state) must each be observable at the spatial and temporal scales of the modelled catchment. Accordingly, the variables of interest are precipitation, surface and root-zone soil moisture, land cover and morphometry, river water-surface elevation, width, slope and discharge, actual evapotranspiration, and soil loss, each of which is now retrievable, to varying maturity, from spaceborne sensors.

The satellite products adopted across these sub-domains span the major Earth-observation families. Precipitation forcing is supplied principally by the Global Precipitation Measurement (GPM) Integrated Multi-satellite Retrievals (IMERG) and the earlier Tropical Rainfall Measuring Mission (TMPA) products; surface soil moisture by the Soil Moisture Active Passive (SMAP), Soil Moisture and Ocean Salinity (SMOS) and Advanced Scatterometer (ASCAT) missions, complemented by AMSR-E and the merged ESA-CCI record. Relief, land cover and morphometry are derived from optical and topographic data; Landsat, Sentinel-2 and MODIS imagery together with SRTM and AW3D30 digital elevation models within a geographic-information-system workflow. Inland hydro-morphology is observed by the Surface Water and Ocean Topography (SWOT) mission and its Ka-band radar interferometer (KaRIn), by Nadir Altimetry (Jason, SARAL and Sentinel-3) and the ICESat-2 photon-counting lidar, and by synthetic-aperture radar (SAR) from Sentinel-1, ENVISAT ASAR and TerraSAR-X. Watershed water storage enters by cross-reference to the Gravity Recovery and Climate Experiment (GRACE/-FO) introduced under climate change in Section 3.1. Among the previous, SWOT is retained throughout this work as the technological centrepiece of the watershed-observation argument, since it measures water-surface elevation, width and slope simultaneously and natively bridges inland and coastal waters (Yao et al., 2025; Biancamaria et al., 2016); the aforementioned “bridge” is developed in Sections 3.3 and 3.4 rather than here.

Regarding weather forcing, satellite precipitation is now used directly as distributed input to rainfall-runoff and hydrological models. Jiang and Bauer-Gottwein (2019) evaluate GPM IMERG across 300 catchments of Mainland China and find the gauge-adjusted final-run estimates to be in good agreement with gauge records at the daily scale and to provide hydrological-model performance comparable to gauge forcing, whereas the older TMPA product performs relatively poorly. Comparable skill is reported across Mediterranean and monsoon settings, with GPM capturing the bulk of the observed precipitation volume over the major Mediterranean islands (Caracciolo et al., 2018) and serving as model forcing elsewhere (Chao et al., 2021). It is noted that, in the most data-poor basins, satellite climatologies can substitute for sparse weather-station networks as the distributed climate forcing of catchment models (Mendelsohn et al., 2007).

Regarding the relief and soil state, surface soil moisture parameterises the antecedent wetness that governs the partition of rainfall between infiltration and runoff. The SMAP mission delivers global surface soil-moisture

and freeze/thaw products that constrain land-atmosphere water and energy fluxes (Entekhabi et al., 2010), and a global triple-collocation assessment ranks SMAP the most skillful of the available retrievals over the majority (~52%) of land pixels, with SMOS and ASCAT each retaining regional advantages (Chen et al., 2018). The dependence of such assessments on adequate ground reference is itself a recognised constraint, since validating coarse satellite products requires the upscaling of sparse in situ observations (Crow et al., 2012). Satellite soil moisture has further been used to set antecedent-condition runoff thresholds on flash-flood-prone Mediterranean basins (Ortenzi et al., 2025), while morphometric and land-cover products parameterise watershed roughness, erodibility and vulnerability. The morphometry, land-use and resilience frameworks synthesised by Nandi et al. (2026) and the land-cover-change records reviewed by Gu and Zeng (2024) are representative works in relevant literature.

Regarding the inland hydro-morphology and water storage, the SWOT mission is the densest single thread of the reviewed literature. Pavelsky et al. (2014) estimate that SWOT could observe rivers wider than ~50–100 m and thereby constrain discharge in more than 60% of river basins larger than ~50,000 km², against fewer than 30% observed by the global gauge network. First-look analyses confirm that SWOT tracks river-discharge dynamics without gauge information, with correct magnitude in many reaches but residual bias in others (Andreadis et al., 2025), while global accuracy assessments report its simultaneous water-level, width and slope retrievals at unprecedented spatiotemporal resolution (Cerbelaud et al., 2025; Yao et al., 2025). The first SWOT river-elevation profiles, demonstrated in the Congo Cuvette Centrale, validate well against nadir altimetry (Normandin et al., 2024); inland water-surface-elevation products have been validated against in situ records in the middle and lower Yangtze River (Zhao et al., 2025) and used, alongside ICESat-2, to diagnose errors in hydraulic models (Charoensuk et al., 2025). Beyond SWOT, river networks and channel morphology are mapped from optical and radar imagery: Li et al. (2024) map 10-m river networks at monthly resolution from Sentinel-1, Sentinel-2 and a 30-m elevation model with an overall accuracy of 95.8%, recovering a Yellow River network of ~40,280 km, roughly 3.2 times the length of earlier Landsat-derived databases. Width-based discharge estimation (Ishikawa et al., 2025), the machine-learning fusion of Sentinel-1 SAR and CYGNSS reflectometry for river water-level monitoring (Jia et al., 2025), gap-filling of cloud-affected fluvial imagery by image warping (Wang et al., 2025) and multi-source actual-evapotranspiration estimation (Wu et al., 2020) further parameterise the routing and water balance of the catchment.

A growing body of work moves beyond observation to the assimilation and calibration of satellite data within the modelling chain (this step is examined in detail in Section 4.1). Joint assimilation of Sentinel-1 SAR and SMAP radiometer observations improves surface and root-zone soil-moisture estimates by ~30% relative to SMAP alone (Lievens et al., 2017); near-real-time assimilation of SAR-derived flood maps sharpens flood forecasts (Hostache et al., 2018); and SAR combined with altimetry reconstructs floodplain inundation dynamics over the Tonle Sap (Chang et al., 2020). Assimilation of satellite soil moisture raises the reliability of agro-hydrological models in large transboundary basins (Eini et al., 2023) and improves coupled water-quality and crop-yield prediction (Pignotti et al., 2023); assimilation of merged satellite precipitation improves flood simulation (Chao et al., 2021); assimilation of SWOT water levels supports near-optimal reservoir operation on the upper Niger (Munier et al., 2015). For calibration, satellite soil moisture and evapotranspiration improve the performance of a large-scale hydrological model (López López et al., 2017), satellite forcing constrains a SWAT model of the Lower Mekong streamflow (Mohammed et al., 2018), and SWOT water-surface elevations calibrate a distributed hydrological model (Patidar et al., 2025). At the assessment level, satellite hydrology: a) supports water-resources decisions where ground data are scarce (Sheffield et al., 2018), b) separates the climate, forest-cover and permafrost drivers of streamflow trends (Duan et al., 2017), c) tracks channel and vegetation response to engineering works and to hydro-climatic variation (Kong et al., 2020; Nones et al., 2024), d) quantifies river

morphological change at scales impractical for field survey alone (Bhattarai et al., 2026), e) reconciles optical and SAR inundation mapping against hydrodynamic models (Ticehurst and Karim, 2023), and f) informs drought-aware water management (Mohammad et al., 2025). Regarding the generation of sediment, satellite-fed empirical erosion models like RUSLE (driven by climate-change scenarios, as in Chakrabortty et al., 2020; Gupta and Kumar, 2017) and the USLE/SCS-CN (characterisation of mountainous watersheds, as in Pareta and Pareta, 2012), translate the land-surface state into the sediment supply that closes the watershed contribution to the coast.

Nevertheless, several limitations remain specific to Component (B). Passive soil-moisture retrievals are delivered at a coarse footprint of ~40 km, far larger than the headwater catchments that often dominate the runoff response, so that sharpening to model resolution depends on radar fusion or assimilation (Lievens et al., 2017), and their validation is constrained by the density of the available ground networks (Crow et al., 2012). For inland waters, SWOT observes only rivers wider than ~50–100 m (Pavelsky et al., 2014), its product accuracy over inland water bodies still requires careful validation (Zhao et al., 2025), and levee-confined or heavily regulated reaches remain harder to characterise (Ishikawa et al., 2025). Optical observation of fluvial change is interrupted by cloud cover and limited revisit, a gap that interpolation methods only partially close (Wang et al., 2025). Finally, it is noted that the most urgent need (which also constitutes the largest residual uncertainty) lies in the data-poor regions; there, in situ monitoring is sparse and satellite information, despite its promise, still contends with issues of accuracy, sampling and continuity (Sheffield et al., 2018; Mendelsohn et al., 2007).

All in all, the satellite observation of watershed dynamics is sufficiently mature to supply Component (B) with forcing, boundary, parameterisation, assimilation, calibration, validation and assessment information across the full range of essential aspects, even where individual products remain uneven in accuracy and coverage. The integration argument turns on SWOT, whose native bridging of inland and coastal waters makes it the connective element between Component (B) and Component (C); that bridge, and the role of SWOT in the river-mouth transition, are developed in the coastal dynamics of Section 3.3 and the transitional zone of Section 3.4, while the watershed-storage parameterisation provided by GRACE/-FO is carried forward from the Climate Change component of Section 3.1 (Tapley et al., 2019; Li et al., 2019). The assimilation and calibration studies grouped above are operationalised in Section 4.1, and the placement of each study by satellite-product family, modelling role and essential aspect is consolidated in the structured matrices of Section 5, where the SWOT and assimilation clusters carry much of the integration argument. The institutional uptake and management of watershed observation are treated separately under Society and Governance in Section 4.3 (e.g. Wang et al., 2016). Accordingly, Component (B) delivers the upstream water and sediment fluxes that set the boundary condition for the watershed–coast coupling of Component (D), to which the following subsections turn.

3.3. Coastal dynamics (Component C)

The satellite data considered in this Section for the Coastal Dynamics (Component C) of a Watershed-Coast System concern three observable domains – marine weather, marine hydrodynamics (waves, currents, sea level variations) and coastal morphology – that together describe the seaward forcing of the system and the morphological response it produces within the methodological framework of Figure 1. Component (C) observes the marine boundary that the watershed fluxes of Section 3.2 meet at the coast; the actual coupling of the two sides at the river mouth is the transitional zone of Section 3.4, and is therefore not treated here. The main variables of interest are the surface wind speed and significant wave height that define the wave climate, the sea-surface height that sets the still-water level, and the nearshore bathymetry (shoreline position and isobaths) that record the morphological change. It is noted that all these observations map to the drivers of

changes in coastal morphology, the essential aspect EA2 of Figure 2 and Table 1, while the multi-decadal trends in wave height and sea level additionally carry the association of those drivers to climate-change scenarios (EA4).

The marine-weather record used in this work is, in the first instance, the multi-decadal satellite-altimetry archive of significant wave height and wind speed. Young and Ribal (2019) analyse an ensemble of 31 satellite missions (13 altimeters, 11 radiometers and 7 scatterometers) over a 33-year period (1985–2018), and report small increases in mean wind speed and wave height with stronger increases in the extreme (90th-percentile) conditions, the largest of them in the Southern Ocean. Confidence in those trends is strengthened by their agreement across the three independent instrument families, and is consistent with the cross-validation of Timmermans et al. (2020), who intercompare significant wave height climatologies and trends over the 1992–2017 period across four global products and against wave buoys. Nevertheless, the latter study is candid that residual discrepancies between altimeter products arise from differences in calibration and quality control, a caveat that limits the unqualified use of any single record. Regarding the regional expression of this variability, Izaguirre et al. (2010) model the seasonal and interannual extremes of the wave climate of southern Europe with a non-stationary extreme-value model tied to the North Atlantic Oscillation and related circulation indices, and Izaguirre et al. (2011) extend the same approach to a global altimeter dataset spanning the period from 1992 onwards. These studies enter the WACS chain as Forcing, i.e. the wave and wind climate that drive coastal morphodynamics, and their multi-decadal trends are the seaward face of the changing climate forcing detailed for Component (A) in Section 3.1. Beyond the altimetry record, Pleskachevsky et al. (2016) retrieve near-real-time significant wave height from X-band synthetic-aperture-radar imagery (TerraSAR-X, ENVISAT and ERS) over the highly variable German Bight, reaching decimetre accuracy and serving primarily to validate operational wave model output.

Two further marine-weather studies use the altimetry record not as direct forcing but to calibrate the wave models that supply it. Reguero et al. (2012) calibrate a third-generation global wave hindcast against satellite altimetry to build the Global Ocean Wave reanalysis spanning the period from 1948 onwards, excluding tropical cyclone outliers and verifying the result against historical measurements; Amarouche et al. (2021) perform the first spatial calibration of the physical parameters of an unstructured SWAN model against seven altimetry missions for the Black and Azov Seas, where wave-buoy coverage is sparse. The former delivers a long and homogeneous wave climatology, the latter a regionally tuned operational model; both belong to the coupling, calibration and validation aspect (EA7) and are revisited as Calibration in the data-assimilation and calibration discussion of Section 4.1.

The sea level record adopted in this work is the satellite-altimetry time series maintained since the early 1990s. Ablain et al. (2017) show that, through improved geophysical corrections and a careful linkage of the reference (TOPEX/Poseidon and Jason) and complementary (ERS, Envisat, SARAL, Sentinel-3) missions, the global mean sea-level trend now approaches the ~0.3 mm yr^{-1} accuracy required by the Global Climate Observing System, with regional trend uncertainty reduced by a factor of ~2; the residual orbital and wet-tropospheric errors are reported candidly as the remaining obstacle near the coast. This record enters Component (C) as Forcing on the still water level. Building on it, Lobeto et al. (2018) present a methodology for estimating return-period extreme sea levels nearshore from altimetry, correcting the remote data with an extreme-scale factor that is defined and validated against tide gauges along the North American east coast; the approach is coded as Parameterisation. It is noted that the native bridging of inland and coastal waters offered by the Surface Water and Ocean Topography (SWOT) mission (Biancamaria et al., 2016), introduced in Section 3.4, carries a

prospective sea-level assimilation role that connects Components (B) and (C); that bridge is drafted in Section 3.4 and operationalised in the matrices of Section 5, and is only cross-referenced here.

The coastal-morphology record used in this work is dominated by the optical satellite-derived shoreline and satellite-derived bathymetry family. At the global scale, Luijendijk et al. (2018) classify 31% of the world's ice-free shoreline as sandy from the Landsat archive and, applying automated shoreline detection over the period 1984–2016, find that ~24% of those sandy beaches are eroding at rates exceeding 0.5 m yr^{-1} while ~28% are accreting and ~48% are stable – a global Assessment of the morphological state of Component (C). At the local-to-coastal scale, Bergsma et al. (2021) demonstrate that spaceborne satellite-derived bathymetry from Sentinel-2, Landsat and VENμS tracks nearshore morphology and validates well against survey data; its extension across the land–sea boundary towards the river mouth is taken up in Section 3.4. High-frequency satellite-derived shorelines resolve beach change and its seasonality (EA6), as Cabezas-Rabadán et al. (2019) show for the Valencian coast (Spain) using dense Sentinel-2 imagery, and operational workflows now detect coastal change automatically across regional coastlines (Gomes da Silva et al., 2024); the same shoreline-extraction principle is established earlier on a decadal Landsat series (Maiti and Bhattacharya, 2011). These applications occupy the Validation role within the family of drivers of changes in coastal morphology (EA2).

Within the same optical family, the morphological detail extracted from the imagery feeds the modelling chain in distinct roles. Janušaitė et al. (2021) automate the detection of nearshore sandbar position, crest and local relief from medium-resolution imagery, parameterising the sub-tidal morphology; the machine-learning satellite-derived bathymetry of Ashphaq et al. (2024) supplies the nearshore depth field as a coastal boundary; the machine- and deep-learning bathymetric mapping of Ngalande and Armenakis (2025) validates depth-range retrievals against in situ data in Canadian coastal waters. Two off-family sensors broaden the same morphological record: the photon-counting laser altimeter ICESat-2, used by Xie et al. (2021) to classify shore-zone morphology, and synthetic-aperture-radar interferometry, used by Marghany (2012) to reconstruct three-dimensional coastal-spit morphology from RADARSAT-1 data (reported coefficient of determination ~0.96). A large cluster of case studies then applies the satellite shoreline record to Assessment: shoreline position is related to interannual meteo-oceanographic forcing in south-eastern Brazil (Carvalho et al., 2020); long- and short-term change dynamics are separated for a Brazilian city coast (Santos et al., 2021); tidal-flat morphology is reconstructed by an optimal-waterline method on the northern coast of Vietnam (Tong et al., 2020); and Arctic shoreline change is assessed by an integrated satellite, field and GIS workflow on Svalbard (Zagorski et al., 2020). Long Landsat time series further quantify estuary-mouth shoreline change (Tsai, 2022) and delimit coastal sediment-cell boundaries through a Monte Carlo shoreline model (Susilowati et al., 2022), whose river-mouth settings are taken up in Section 3.4. The same record supports coastal-vulnerability and coastal-risk characterisation (Cenci et al., 2017; Gómez et al., 2014), which connects the morphological signal to the ecological and socio-economic implications (EA5) discussed in Section 4.2, and it links beach morphodynamics to the accumulation of *Posidonia oceanica* wrack detected from imagery (Terracciano et al., 2026).

Regarding the limitations specific to Component (C), the satellite records described above are constrained by the coastal margin itself. Conventional nadir altimetry degrades within ~10–20 km of the shore, where the radar footprint is contaminated by land and the along-track sampling is too coarse to resolve the nearshore gradient, and the inter-mission calibration and quality-control differences noted by Timmermans et al. (2020), together with the residual orbital and wet-tropospheric errors reported by Ablain et al. (2017), place a floor on the achievable regional accuracy. The optical satellite-derived shoreline and bathymetry products are limited by cloud cover and revisit interval, by the water turbidity that attenuates the bottom-reflected signal (this difficulty is made explicit for the turbid Indian coastline by Ashphaq et al.,2024), and by the tidal-stage ambiguity of any

single waterline, which Tong et al. (2020) address only by combining many acquisitions into a multi-temporal solution. It is noted, further, that the off-family synthetic-aperture-radar and laser-altimeter retrievals remain largely one-off demonstrations rather than systematically assimilated inputs to a coupled model.

All in all, the satellite observations of Component (C) populate the seaward half of the WACS chain of Figure 1 in a consistent and complementary way. The multi-decadal altimetry record of wave height and sea level supplies the Forcing and Boundary conditions (wave climate, sea level variations and their changing-climate trends) that the watershed fluxes of Section 3.2 meet at the coast, while the optical satellite-derived shoreline and bathymetry family supplies the morphological response against which coupled models are calibrated and validated (Section 4.1) and from which ecological and socio-economic implications are assessed (Section 4.2). The native SWOT bridge between inland and coastal waters (Biancamaria et al., 2016) and the satellite-derived shoreline data assimilation of Vitousek et al. (2023) are the explicit hand-offs to the watershed side and to the assimilation discussion of Section 4.1, respectively. The river-mouth coupling that joins the two components, i.e. the land-to-sea morphology products, the satellite suspended-sediment signal and the shoreline–fluvial interaction, is the transitional zone of Section 3.4. Accordingly, the placement of each study by product family, modelling role and essential aspect is carried forward into the structured framework of Section 5.

3.4. Integration of the Watershed-Coast System: the transitional zone (Component D)

The transitional zone examined in this Section is the river-mouth, estuary and delta interface at which the watershed fluxes of Section 3.2 and the coastal forcing and response of Section 3.3 meet and couple, and which Samaras (2023) places at the integration core of the Watershed-Coast System as Component (D) (see Figure 1). Conceptually, the watershed, the transitional zone and the coast form three contiguous regions, with the transitional zone bounded between them and a channel network crossing all three and rejoining the sea as a sediment plume. The variables that must be observed across this envelope are precisely those that the two flanking components hand over to one another: the river-mouth water and suspended-sediment discharge that Section 3.2 delivers as the watershed boundary (essential aspect EA1 of Figure 2 and Table 1), the topography–bathymetry continuum and the shoreline position that Section 3.3 tracks as coastal morphology (EA2), and the water-surface elevation and vertical land motion that reference the two to a common datum. It is noted that this zone is, at once, the most data-poor in situ (gauges and bathymetric surveys are sparse, costly and frequently interrupted at turbid, shifting river mouths), the most geomorphologically dynamic, and the operational locus of the coupling (EA6 and EA7) that defines Component (D). Accordingly, satellite observation acquires a value here that it does not carry over either flanking component alone, because it supplies the only spatially continuous, repeat record of an interface that in situ networks systematically under-sample.

The technological spine of this coupling is the Surface Water and Ocean Topography (SWOT) mission, the named centrepiece of the integration argument advanced in this work. Biancamaria et al. (2016) describe SWOT as both a continental-hydrology and an oceanography mission, and it is this dual design that makes it the native bridge between Components (B) and (C): a single KaRIn swath measures river stage, width and the surface-water slope from which discharge is inferred on the landward side, and sea-surface height on the seaward side, across the same river-mouth scene. The landward measurement is the river-mouth discharge boundary that Component (D) hands to a coastal model (EA1); the seaward sea-level measurement supports the assimilation prospect already set out, on the Component (C) side, in Section 3.3. The mission was a forecast at the time of Biancamaria et al. (2016) and is now an observation. Lichtman et al. (2025) evaluate SWOT total water levels through the hyper-tidal Bristol Channel–Severn Estuary (UK), one of the most dynamically complex coastal zones globally, and report that the Level-3 product, once a water-elevation-dependent offset is removed, is in

good agreement with a network of in situ gauges, with root-mean-square differences of ~0.14 m (these values are comparable to the 0.17 m obtained for CryoSat-2). The two-dimensional water-level maps resolve fast, kilometre-scale spatial patterns from the river, through the estuary, to the open sea – exactly the spatial transition that the one-dimensional nadir altimetry of Section 3.3 cannot image. Building on the same family, Payandeh et al. (2026) assemble a fully satellite-driven workflow for a data-scarce coastal lagoon in which no local in situ measurement is used at all: a satellite-derived bathymetry, trained on Sentinel-2 reflectance against ICESat-2 photon depths, reproduces independent reference points with a root-mean-square error of 0.45 m and a coefficient of determination $R^2 = 0.97$, and the resulting hydrodynamic model is validated against sixteen SWOT passes. Regarding the model coupling itself, the satellite data are set up here as the boundary and validation of Component (D), while the coupled modelling is taken up in Section 4.1 and the placement of the SWOT cluster by product family, modelling role and essential aspect is operationalised in the matrices of Section 5.

The topography–bathymetry continuum, that is the legitimate sub-domain of Component (D) that Section 3.3 deferred to here, is the second product thread. Caballero and Stumpf (2019) provide a clean demonstration of optical satellite-derived bathymetry, retrieving nearshore depths from the Sentinel-2A and 2B MultiSpectral Instrument through a ratio-transform model: in clear South Florida waters the retrieval reproduces chart depths with a median absolute error of 0.22–0.5 m across the 0–18 m range, the 10 m instrument captures tidal channels and steep slopes, and a generic, scene-independent calibration degrades the error only moderately, to a median of ~1 m. It is noted that this performance is conditional on low turbidity, a constraint that emerges as most significant at sediment-laden river mouths. Where clear-water optics fail, two complementary routes carry the continuum. Capo et al. (2014) reconstruct the decadal morphodynamic evolution of a mixed-energy tidal inlet from a ~26-year archive of 78 optical scenes, characterising flood- and ebb-tidal-delta migration at a seasonal cadence that field survey cannot match; and Li et al. (2023) use five years of Sentinel-1 interferometry, with ICESat-2 elevations, to map coastal subsidence over the Yellow River Delta, resolving fast-subsiding funnels exceeding 50 mm yr^{-1} and a maximum rate above 300 mm yr^{-1} that revises the delta's inundation scenarios. Munasinghe et al. (2021) survey the field as a whole, comparing eighteen satellite techniques for delta-morphology change and finding sub-pixel methods to outperform pixel-based ones, with unsupervised classification recommended as a first-order extraction in data-sparse deltas. The nearshore satellite-derived bathymetry and waterline studies that anchor this continuum on the open-coast side are placed in Section 3.3 (Bergsma et al., 2021; Ashphaq et al., 2024; Tong et al., 2020; Tsai, 2022) and are drawn on here only where the land–sea topography–bathymetry handover is the point.

The third thread is the suspended-sediment signal at the river mouth, the satellite observable that most directly carries the Section 3.2 watershed flux across the interface (EA1). Beveridge et al. (2020) lead this cluster with a cloud-based tool that maps estimated suspended-sediment concentration over optical imagery and returns long-term concentration time series at user-chosen points along major Bangladesh rivers, providing the river-mouth sediment-discharge boundary where conventional gauging is sparse; the stakeholder-engagement and communication dimension of the same tool is a Society-and-Governance topic taken up in Section 4.3. The seasonal-to-interannual behaviour of this flux is resolved by Gensac et al. (2016), who track suspended particulate matter from ocean-colour imagery along the 1500 km Amazon-to-Orinoco coast and attribute the mud-bank shoals at the river mouth to the Amazon water and sediment discharge, which accumulate during high discharge and are flushed seaward at the discharge peak. At the global scale, Hou et al. (2024) examine coastal suspended-sediment concentration and river-plume area for 349 deltas from two decades of optical imagery (2000–2020); they report a sustained mean increase of +0.46% and +0.48% yr^{-1} respectively, present on every continent except Asia, although as many as 45.2% of deltas show concentration trends opposing their

river-sediment trend under the modulating influence of tides, waves, salinity and delta morphology. The watershed inflow that these river-mouth signals receive (i.e. the fluvial water and sediment characterised by the inland studies of Section 3.2: Andreadis et al., 2025; Kong et al., 2020; Normandin et al., 2024) is the boundary that closes the watershed-to-mouth handover. The implications of the deltaic-change signal for wetland resilience and the exposure of delta populations point forward to the changing-climate forcing of Section 3.1 and the ecological and socio-economic discussion of Section 4.2 (EA8).

Where the suspended-sediment thread observes the flux, the shoreline–fluvial cluster observes its morphological consequence: the position of the coastline and the migration of the channel that feeds it. Cui and Li (2011) provide the canonical case, extracting mean-high-tide lines of the Yellow River estuary from Landsat MSS, TM and ETM+ imagery over 1976–2005 and partitioning the record into rapid-accretion, adjustment, slow-erosion and slow-accretion stages governed by the river's runoff and sediment load; they further estimate the critical annual runoff and sediment load of 140.36 × 10^8 m^3 yr^{-1} and 3.31 × 10^8 t yr^{-1} required to hold the estuary in balance, an explicitly coupled watershed-to-coast statement. The same coupling is read at other deltas. George et al. (2019) map the fluvial, tidal and wave-dominated environments of the 70,000 km^2 Niger Delta from Landsat and SPOT imagery, partitioning it into upper-deltaic-plain, lower-deltaic-plain and delta-front units that occupy 69%, 25% and 6% of the extent; Bhaskar and Kumar (2011) read river migration from coastal geomorphology in southern India; and Sufyan et al. (2025) interpret a Landsat time series of the Porong estuary (Indonesia) alongside a sediment-transport model, the satellite record showing the Lusi Island land area expanding from 6.29 ha in 2000 to 147.86 ha in 2024. It is noted that the model coupling in the latter study is set up here through the satellite waterline observation and is carried into Section 4.1. Gómez et al. (2021) add the vertical dimension that the planimetric shoreline alone omits, combining optical imagery with synthetic-aperture-radar interferometry to show, on a Colombian Caribbean delta over 2007–2021, that subsidence rates of up to 1.0 cm yr^{-1} coincide with shoreline erosion of up to 15 m yr^{-1} – while erosion also occurs where no subsidence is detected, so that vertical land motion is one driver among several. The satellite-derived-shoreline tooling on which this cluster rests is the canonical CoastSat workflow of Vos et al. (2019), the shoreline backbone of this Section, which extracts shorelines from more than thirty years of publicly available Landsat and Sentinel-2 imagery and resolves shoreline variance well at timescales of six months and longer, with cross-shore accuracies of 7.3–12.7 m against field survey; its assimilation into predictive shoreline models is taken up in Section 4.1 (Vitousek et al., 2023).

Several limitations are specific to this zone rather than to the sensors in general. Regarding the optical thread, the clear-water assumption that underpins satellite-derived bathymetry and ocean-colour suspended-sediment retrieval is least valid exactly where Component (D) is most active: the turbid, cloud-prone plume at a working river mouth degrades both depth retrieval (Caballero and Stumpf, 2019) and concentration inversion, and the shoreline itself is a tide-, surge- and runup-dependent instantaneous feature whose definition carries an irreducible cross-shore uncertainty (Vos et al., 2019). The interferometric thread is constrained to coherent surfaces and resolves vertical motion rather than the bed itself (Li et al., 2023; Gómez et al., 2021). The swath-altimetry thread, although transformative, is young and relatively unexplored: the SWOT record evaluated by Lichtman et al. (2025) derives from the calibration–validation phase, and the nearshore comparison requires correction of an elevation-dependent offset before the gauge agreement is recovered. It is noteworthy, though, that these are localised qualifications on an otherwise decisive gain in coverage; the deeper friction is one of representation rather than accuracy. Two studies in this Section carry sensors that sit outside the seven product families on which the framework's by-product axis is built – ICESat-2 photon altimetry within the multi-sensor stacks of Payandeh et al. (2026) and Li et al. (2023), and synthetic-aperture-radar interferometry for vertical

land motion (Li et al., 2023; Gómez et al., 2021). Their placement on that axis is examined where it belongs, at the construction of the structured matrices in Section 5, rather than reopened here.

All in all, the transitional zone is where the four components of the Watershed-Coast System cease to be a list and become a chain, and the satellite record is what makes the links observable. The river-mouth discharge and suspended-sediment boundary of EA1, handed forward from the watershed of Section 3.2, and the topography–bathymetry continuum and shoreline response of EA2, handed back from the coast of Section 3.3, are not merely co-located here; they are jointly measured, increasingly by a single mission. SWOT is the concrete instrument of that joining: as Biancamaria et al. (2016) anticipated and Lichtman et al. (2025) now demonstrate, one swath references the landward and seaward water surfaces to a common two-dimensional field, and Payandeh et al. (2026) show that, together with satellite-derived bathymetry, it can drive and validate a coastal hydrodynamic model with no in situ measurement at all. The role of the present Section is to supply and characterise these data at the interface; the coupling, calibration and validation that consume them (i.e. the EA7 core of Component D) are the subject of Section 4.1, and the placement of each study by product family, modelling role and essential aspect is operationalised in the structured matrices of Section 5, with the family-level fingerprint previewed in Figure 3. It is on this basis that the Discussion of Section 6 frames a SWOT-era opening for integrated Watershed-Coast System modelling: the transitional zone, long the data-poorest link in the chain, is becoming the one most directly served by the satellite observing system.

4. Satellite data for WACS integration and decision-making

4.1. Coupling, calibration and validation: the integration mechanisms

The integration of the satellite observations characterised in Section 3 into the modelling of Watershed-Coast System morphodynamics, examined in this Section, proceeds through four mechanisms by which an observation enters a model: as a boundary condition or forcing, as a state or parameter update through data assimilation, as a calibration target, and as the validation of a past or present system state. Whereas Section 3 established what the satellite record observes across the four components, this Section establishes how that record is consumed by a model, and it is here that Samaras (2023) places essential aspect EA7 – the coupling, calibration and validation of the integrated chain, including the decision on a model's appropriate complexity (Figure 2). The observations are not re-described here: each is back-referenced to the component Section that supplies it, and the unit of discussion is the modelling step. Of the four mechanisms, data assimilation carries the densest and most load-bearing evidence, calibration follows, and the forcing and validation threads are largely received from Section 3 with a few exemplars.

Regarding the lightest of the four mechanisms, the satellite sea level and wave climate of Section 3.3 and the precipitation and river discharge of Section 3.2 enter coastal and watershed models as forcing and boundary conditions, and the present Section draws on this thread only through a small number of exemplars in which the satellite product is the explicit model input. Chao et al. (2021) merge several satellite precipitation estimates with gauge data and use the blended field to force the WRF-Hydro-RAPID model, the improved-quality forcing raising flood-simulation accuracy in a Yangtze sub-basin where the individual raw products are too coarse. On the seaward side, the water-surface elevation continuum of the Surface Water and Ocean Topography (SWOT) mission, characterised in Section 3.4 as the native bridge between Components (B) and (C), supplies the river-mouth discharge boundary that Component (D) hands to a coastal model (EA1); its consumption as an assimilation target, rather than as a static boundary, is taken up below.

The assimilation of satellite data into watershed, coastal and morphodynamic models is the mechanism that most distinguishes this Section from a catalogue of observations, and it is led here by the study coded primary to Section 4.1. Vitousek et al. (2023) assimilate the satellite-derived shorelines of Section 3.4 (i.e. the CoastSat-type record extracted from three decades of Landsat and Sentinel-2 imagery) into an ensemble shoreline change model spanning the ~1,760 km California coast, and report a forecast root-mean-square error below 10 m over nearly half of that coast for an independent 2015–2020 validation period. The same study supplies the load-bearing calibration result of this Section: calibrating the shoreline model on satellite-derived shorelines yields forecast skill nearly equivalent to calibrating on monthly in situ surveys, so that the satellite record substitutes for the field-survey network that does not exist at continental scale. The SWOT assimilation thread, foreshadowed in Section 3.4, is the integration centrepiece. Biancamaria et al. (2016) set out the prospect of assimilating SWOT water-surface elevations into hydrodynamic and hydrology models to correct their state vectors or parameters within an observing-system-simulation framework. They note candidly, though, that for some flood events, modelling error outgrows the initial-condition error within days and the assimilation benefit dissipates. Munier et al. (2015) provide the concrete demonstration: an ensemble Kalman filter assimilating virtual SWOT water levels into a coupled hydrodynamic–reservoir model on the Upper Niger (Mali) improves both the simulated water level and the downstream discharge, the benefit persisting longer when a Kalman Smoother is applied.

Beyond the shoreline and SWOT threads, the assimilation literature clusters by the satellite observable that updates the model. Several studies assimilate satellite soil moisture into distributed hydrological models: Chen et al. (2011) update the surface layer of the SWAT model with surface soil moisture through an ensemble Kalman filter, but find that the model's limited vertical coupling transmits the update only weakly to the deeper layers and that the real-data experiment is largely unsuccessful at improving streamflow. Lievens et al. (2017) jointly assimilate Sentinel-1 backscatter and SMAP brightness temperature, finding that the addition of the radar increases the assimilation impact on soil-moisture accuracy by up to ~30% relative to SMAP alone. Pignotti et al. (2023) assimilate SMAP surface soil moisture into SWAT and trace its propagation to water-quality and crop-yield predictions, the socio-economic dimension of which is taken up in Section 4.2. The terrestrial-water-storage signal that couples Components (A) and (B) is assimilated from gravimetry: Zaitchik et al. (2008) assimilate GRACE storage anomalies into a land-surface model over the Mississippi basin with an ensemble Kalman Smoother, improving the simulated groundwater variability and raising the correlation of modelled storage with gauged river flow in seven of eight sub-watersheds, while Li et al. (2019) extend GRACE assimilation to the global scale for groundwater and drought monitoring. The flood-inundation thread is carried by synthetic-aperture radar: Hostache et al. (2018) sequentially assimilate probabilistic flood maps derived from ENVISAT ASAR and TerraSAR-X imagery into a flood-forecasting cascade in near-real time, improving the water-level forecast with a benefit that persists from hours to days, and Chang et al. (2020) integrate Sentinel-1 radar and Jason altimetry to reconstruct and forecast daily inundation extents over the Tonle Sap floodplain. It is noted that the two synthetic-aperture-radar studies draw on sensors that sit outside the seven product families on which the framework's by-product axis is built, and their placement on that axis is examined at the construction of the matrices in Section 5 rather than reopened here.

Regarding calibration, the satellite record provides the reference against which model parameters are tuned where in situ data are sparse, and the thread is led by the wave-climate reanalysis on the coastal side. Reguero et al. (2012) calibrate the hindcast of the Global Ocean Wave reanalysis against multi-mission nadir altimetry (the altimetric significant wave height of Section 3.3) excluding tropical-cyclone outliers and then validating the calibrated product against the same satellite record in space and time. Amarouche et al. (2021) carry the approach to the regional scale, performing a spatial calibration of SWAN (spectral wave) model results against

significant wave height from seven altimetry missions over the Black and Azov Seas. On the watershed side, the calibration target is most often satellite soil moisture, evapotranspiration or precipitation: López López et al. (2017) calibrate a large-scale hydrological model against satellite soil-moisture and evapotranspiration products and obtain reasonable discharge skill, with Nash–Sutcliffe efficiencies of ~0.5–0.75, although the agreement remains below that achieved by calibration on in situ streamflow. Eini et al. (2023) add satellite soil moisture as a second calibration objective alongside discharge in the SWAT+ model over the transboundary Odra basin (Poland and Germany), improving the spatial reliability of the simulated runoff, while Mohammed et al. (2018) calibrate the SWAT model with satellite precipitation to examine streamflow variability in the Lower Mekong. The SWOT calibration thread closes the set: Patidar et al. (2025) convert SWOT-derived water-surface elevations to discharge and use them to calibrate a distributed hydrological model over the Indian region, the satellite-proxy discharge yielding a calibration skill approaching that obtained from in situ records.

The validation of past and present Watershed-Coast System states rests on the accuracy of the satellite products themselves, and is therefore received largely from the observational Sections, qualified by two threads. Ablain et al. (2017) reprocess ~25 years of satellite altimetry into a sea level climate record, reducing the regional trend uncertainty by roughly a factor of two and bringing the global mean sea level record towards the ~0.3 mm yr^{-1} stability target of the Global Climate Observing System – the accuracy on which the use of altimetry as both forcing and validation depends. Nevertheless, the satellite products do not all agree, and validation against them is not a solved problem: Timmermans et al. (2020) intercompare global significant wave height climatologies and trends across altimetry and reanalysis datasets and find broad agreement in spatial pattern but substantial divergence in the equatorial belt and the Indian Ocean, attributable to differences in inter-mission calibration and quality control. The SWOT-era coupling exemplars that Section 3.4 forward-pointed to close the mechanism. Lichtman et al. (2025) validate SWOT total water levels across the river-to-open-sea continuum of a hyper-tidal estuary against a gauge network, recovering root-mean-square differences of ~0.14 m once a water-elevation-dependent offset is removed. Payandeh et al. (2026) close the loop with a fully satellite-driven coastal hydrodynamic model, in which a satellite-derived bathymetry supplies the boundary and SWOT passes supply the validation with no in situ measurement. Sufyan et al. (2025) drive and interpret a Delft3D estuary morphodynamic model against a Landsat-derived shoreline series, the satellite record tracking the land expansion that the coupled model reproduces. In each case the data are characterised in Section 3.4, while only the coupled-modelling step is drafted here.

All in all, the four mechanisms show that the satellite record now enters the Watershed-Coast System modelling chain at every stage – from forcing, through assimilation and calibration, to validation – and increasingly informs the EA7 decision on a model's appropriate complexity. The global coverage of satellite-derived shorelines justifies a reduced-complexity shoreline ensemble across continental coasts that no field network could calibrate (Vitousek et al., 2023), while the two-dimensional water-surface continuum of SWOT justifies the coupled hydrodynamic modelling of Component (D) in estuaries that in situ networks systematically under-sample (Lichtman et al., 2025; Payandeh et al., 2026). It is noteworthy, though, that one link remains weakly served: the river-mouth suspended-sediment flux that closes the watershed-to-coast coupling is now well observed, yet it is seldom assimilated into, or used to calibrate, a coupled morphodynamic model. The latter is the persistent, satellite-data-enabled sediment-flux-coupling gap that the Discussion of Section 6 takes up alongside the scale-matching and SWOT-era threads. The socio-economic and communication implications of these integrated chains (EA5 and EA8) are the subject of Sections 4.2 and 4.3, and the placement of each study by product family, modelling role and essential aspect is operationalised in the structured matrices of Section 5, in which this coupling–calibration–validation aspect is the densest of the integration aspects.

4.2. Assessment of ecological and socio-economic implications

The assessment examined in this Section is the reading of modelling results for their ecological and socio-economic implications, the downstream end of the Watershed-Coast System chain at which the coupled and validated model state of Section 4.1 is translated into consequences for ecosystems, coastal communities and water resources. It is useful to distinguish the inward-facing analysis that produces that state from the outward-facing assessment that interprets it, and it is the latter direction (i.e. observation, to model, to implication) that defines the essential aspects EA5 and EA8 of Figure 2: the association of drivers, and of modelled future states, to ecological and socio-economic implications. It is noted that the studies gathered here use satellite data not to improve a model but to read a result, and accordingly they are discussed by assessment target rather than by product family, with their placement by family, role and aspect deferred to the structured matrices of Section 5.

The first assessment target is the socio-economic exposure that follows coastal change. Hassan and Rahmat (2016) read the consequence of a measured shoreline retreat for the resident community at Batu Pahat, Malaysia, combining topographic maps from 1985 with satellite imagery from 2011 and 2013 and a Coastal Vulnerability Index to locate the populations at risk, and trace the loss of land and the destruction of cash crops to a direct reduction in agricultural income. The same socio-economic reading is made at the regional scale by Ndour et al. (2018), who derive shoreline-change rates from satellite data along the developed coasts of Senegal and Benin and attribute an average post-breach erosion of 3.72 m yr^{-1} along the Langue de Barbarie spit, at the mouth of the Senegal River, to the artificial breaching of 2003, with consequences for a densely inhabited and historically significant coastal zone. Regarding both studies, the shoreline observation rests on the coastal-monitoring methods characterised in Section 3.3, whereas the contribution read here is its translation into community exposure (EA5).

The second target is the ecological implication, read increasingly through the lens of nature-based solutions. Heerma van Voss and Ouellette (2024) provide a national-scale proof of concept, processing cloud-based satellite data against biophysical, pedological, hydrological and climatological criteria to map the suitability of eight nature-based-solution types across Rwanda and Lesotho, and converting the resulting spatially explicit layers into marginal abatement cost curves that place an ecological assessment directly in front of a financing decision. At a larger extent, Ma et al. (2026) construct one-kilometre anthropogenic-activity and ecological-condition indices for China over the 2000–2020 period and find that 69.94% of the territory underwent synchronous human–nature change; this finding challenges the assumption of a decadal ecological lag and identifies the Hu Line as a governance-capacity threshold across which institutional effectiveness, rather than pressure alone, separates coordination from conflict. It is noted that both studies read satellite indicators as a statement about ecological state and its governance rather than as a model input (exactly the EA5 association of drivers to ecological implications).

The third target, received from the coastal monitoring of Section 3.3, is the characterisation of vulnerability and risk. Cenci et al. (2017) carry a Landsat shoreline record from the mid-1980s to 2011 forward into a validated three-year predictive scenario for two contrasting coasts; based on their findings they emphasise that the assessment of uncertainty is decisive once such outcomes enter coastal risk management, although admitting that their applied method proved most reliable on higher-energy, non-urbanised coastlines. Gómez et al. (2014) read a comparable Landsat record of the Outer Hebrides over the 1989–2011 period with the Digital Shoreline Analysis System (DSAS), reporting low mean change of ~0.3 m yr^{-1} for the vegetation limit but locally high progradation and erosion of up to 2.5 m yr^{-1}, and conclude that the satellite record supports the

characterisation of geomorphologically dynamic coasts at regional scales. Regarding both, the shoreline observation belongs to Section 3.3; the step read here is its conversion into a vulnerability and risk statement (EA2, EA5).

The fourth target moves inland to water resources, drought and water quality, received from the watershed observation of Section 3.2 and the assimilation of Section 4.1. Mohammad et al. (2025) analyse a Landsat record of the groundwater-dependent Azraq basin in eastern Jordan from 1990 to 2024 through the normalised difference moisture and water indices, and read a consistent decline in surface moisture, marked after 2000, as a decision-support signal of hydrological deficit for sustainable water management (EA1, EA5). The socio-economic facet of the SMAP soil-moisture assimilation of Section 4.1 is read here through Pignotti et al. (2023), whose assimilation, set up and validated in that Section, is shown to propagate into materially different water-quality and crop-yield predictions (i.e. the EA8 consequence of a modelled state for agriculture and water quality) rather than into streamflow alone. Accordingly, satellite assessment is most valuable exactly where in situ measurement is weakest, and the Section closes on that motivation: Sheffield et al. (2018) review satellite remote sensing for water-resources management in data-poor regions and find it generally underutilised yet positioned, with the new mission generation, to transform management where ground networks are sparse – a Society-and-Governance theme carried forward to Section 6.

4.3. Stakeholder engagement and communication

The communication examined in this Section is the use of satellite data as a stakeholder-facing artefact; this regards the visualisations, web portals, co-developed monitoring systems and citizen-science instruments through which an observation or a modelled result reaches the people who act on it – together with the failure modes of that use. This is the concrete realisation of the Science–Society–Governance bridge introduced in Section 2 (Fig. 6 in Samaras, 2023), and it operationalises the same essential aspects, EA5 and EA8, on their communication rather than their assessment side. Accordingly, the studies are discussed by mechanism.

The first mechanism is stakeholder engagement and co-developed monitoring. Quinn et al. (2022) survey the use of geographic information systems and remote sensing across the watershed-planning process and argue that the growing accessibility of these datasets must be matched by inclusive, participatory engagement if management solutions are to hold. The clearest worked example is the suspended-sediment tool of Section 3.4. Beveridge et al. (2020), whose observation belongs to that Section, report that the value of the tool lay less in the imagery than in the engagement process, meaning the partnership and trust between researchers and the Bangladesh Water Development Board, stakeholder leadership and ownership, and an open-source, easy-to-use design. Based on this the aforementioned study draw the general lesson that environmental decision-support tools fail in society when they are *user-inspired* rather than *user-ready*. The same emphasis on indicators, regular review and explicit communication tools recurs in the adaptive-management work of Zuniga-Teran et al. (2022) at the Cienega Watershed (USA), and in the review of successful coastal-management applications by McCarthy et al. (2017), both of which treat the satellite product as one input to a stakeholder process rather than an end in itself (EA5, EA8).

The second mechanism makes that failure mode its explicit subject: the gap between a tool that is *user-inspired* and one that is *user-ready*. Surveys of user needs and uptake converge on it from several directions, starting from the engagement of water-quality managers with Earth observation (Agnoli et al., 2023), to the land-use and land-cover information needs of Brazilian institutions (Cerbaro et al., 2020), and to the enablers and barriers that shape adoption of satellite data by European local and regional authorities (Filippi and Aiello,

2025). It is noted that the common finding is not a deficit of data but a deficit of fit between the data and a ready user.

The third mechanism, citizen science, addresses the deficit of coverage from the demand side. Busch et al. (2016) examine phytoplankton dynamics in a north-west Mediterranean aquaculture zone where ocean-colour retrieval degrades close to the coast, and show that observations contributed by citizens through the Citclops smartphone application, which simplifies water colour to the twenty-one hues of the Forel-Ule scale, agree well with in situ radiometry and complement ocean-colour imagery, extending the spatio-temporal coverage of the satellite record (EA5).

The fourth mechanism is the framing of satellite data for policy and governance, where the artefact is institutional rather than technical. De Leeuw et al. (2010) set the terms in a review of remote sensing in support of environmental policy, finding that the relevant literature had grown faster than remote sensing as a whole yet that almost none of more than three hundred peer-reviewed papers documented actual policy support; this is an early statement, at the level of policy, of the same gap between *user-inspired* and *user-ready* work. Around this anchor, satellite data are read as a governance instrument in several settings: the changing politics of transboundary water, where shared observation can either defuse or inflame conflict over international river basins (Gleason and Hamdan, 2015); the under-acknowledged contribution of space-based Essential Climate Variables to European climate policy (Poirier et al., 2024); the emergence of collaborative "social forestry" tracked through time-series satellite and inventory data in Oregon (Gosnell et al., 2020); and the integration of satellite data with watershed modelling into a geospatial-governance workflow for water resources (Jimenez et al., 2025). Framing the practice without reference to a specific mission, three conceptual studies position it in the wider governance literature: the evolution of integrated watershed management (Wang et al., 2016), the emergence of data-driven anticipatory governance (Maffei et al., 2020), and the consequences of how resilience is framed for the governance of coastal social-ecological systems (Clement et al., 2023). These three studies are read here as the governance scaffold into which the observational studies report (EA5).

All in all, Sections 4.2 and 4.3 complete the downstream half of the Watershed-Coast System chain: where Section 4.1 couples and validates the model, these Sections read its results for ecological and socio-economic meaning and carry them across the Science–Society–Governance bridge to the stakeholders who act on them. The recurring lesson is that the bridge is not crossed by the satellite product alone; the same gap between *user-inspired* and *user-ready* provision surfaces at every mechanism: in co-developed tools, in user-needs surveys, in citizen science and in policy framing. It is this gap, together with the promise of satellite assessment in the data-poor regions where it is most needed, that the Discussion of Section 6 takes up as the cross-cutting Society-and-Governance theme, while the placement of each EA5 and EA8 row by product family, modelling role and essential aspect is operationalised, with the rest of the corpus, in the structured matrices of Section 5.

5. A structured framework for the use of satellite data in Watershed-Coast System modelling

The structured framework proposed in this work is presented as the "twin" matrices of Figures 3 and 4 that place every coded work at the intersection of an essential aspect, a satellite product family and a modelling role, qualified by its spatial and temporal scale. The row axes are the set of eight essential aspects (EA1–EA8) through which Samaras (2023) systematises the path from observation to informed decision-making (Section 2, Figure 2); the column axes are read in two complementary views over the same coded corpus of 113 works and 119 rows. Figure 3 presents the by-product view, in which the seven satellite product families form the columns and each cell records the modelling roles that the family plays for that aspect together with the

dominant scale; Figure 4 presents the by-role view, in which the eight modelling roles form the columns and each cell records the product families that act in that role. The two views are not independent figures but two pivots of one assignment: a work that supplies, for example, a SWOT water-surface elevation as a river-mouth boundary for the coupling aspect occupies the SWOT column of Fig. 3 and the Forcing column of Fig. 4 at the same EA1 and EA7 rows.

It is noted that the Boundary role, which carries the Component (D) river-mouth handshake set out in Section 3.4, is coded in full but folded into the Forcing column for display and tagged *:b*, so that no assignment is lost on the pivot. The by-product pivot totals 190 (paper × role × aspect) contributions and the by-role pivot 211; the two differ by the 21 contributions of works whose sensors fall outside the seven product families, addressed at the close of this Section.

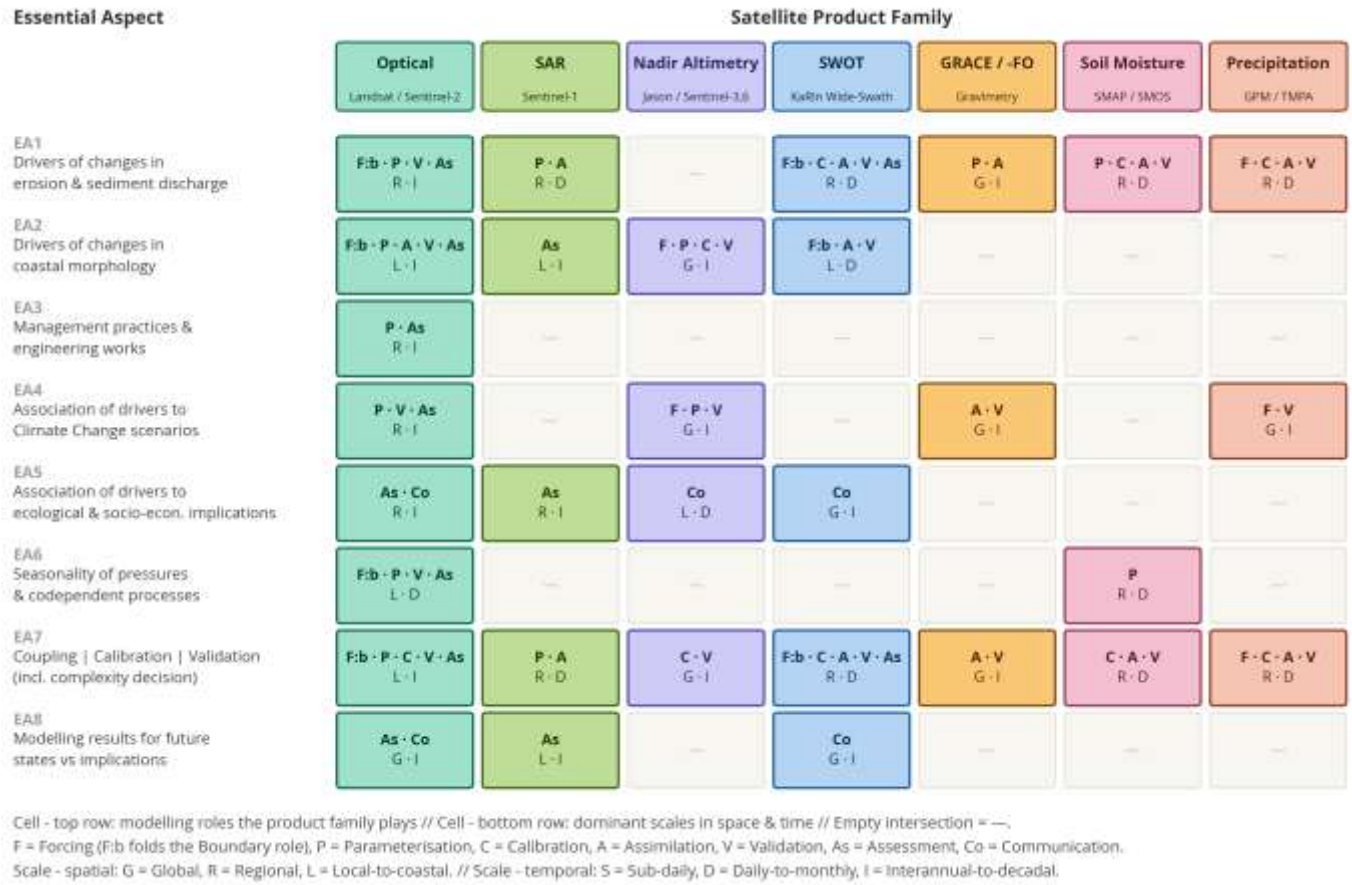


Figure 3. Structured-framework matrix, by product family: eight essential aspects (EA1–EA8) × seven satellite product families; cell tokens denote the modelling roles and the dominant scale. EA1–EA8 (rows) are defined in Table 1.

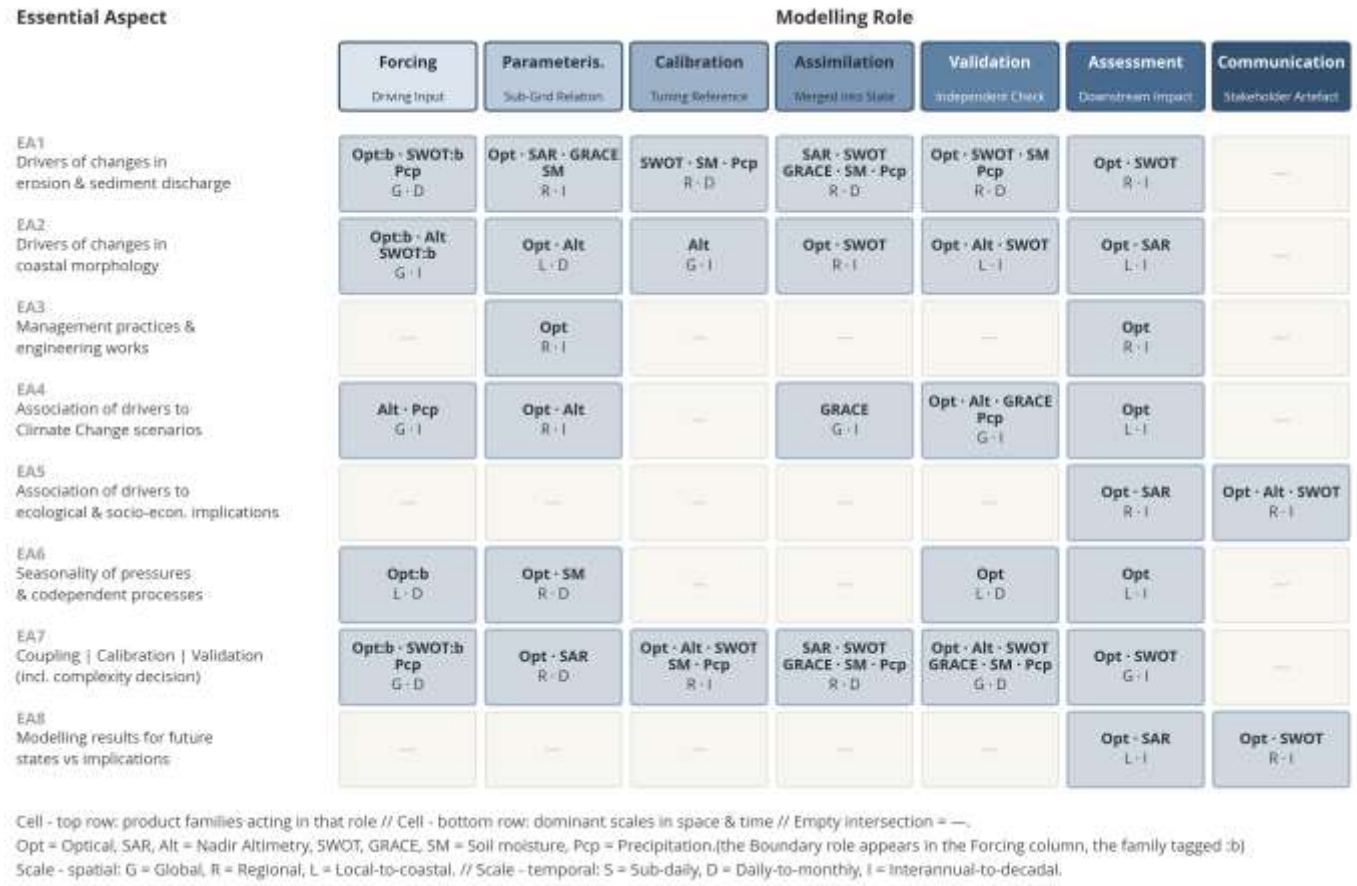


Figure 4. Structured-framework matrix, by modelling role: eight essential aspects × seven modelling roles; cell tokens denote the product families and the dominant scale. EA1–EA8 (rows) are defined in Table 1.

Figure 5 shows the density of the corpus across the same two pivots; in it, cell intensity scales with the number of coded works and the row and column totals are carried in the neutral-grey margin. Among the product families, the optical record dominates the literature by a wide margin, with 94 of the 190 by-product contributions, and it is the only family present in all eight essential aspects (Fig. 5, left panel). The Surface Water and Ocean Topography (SWOT) mission is the second most represented family at 29 contributions (a notable position for a mission launched only in late 2022) while the remaining families occupy more specialised niches: Nadir Altimetry (18), the Precipitation constellations (15), Soil Moisture (14), SAR (12) and GRACE gravimetry (8). Regarding the modelling roles, the downstream Assessment role is the most populated at 52 contributions and Validation follows at 44 (Fig. 5, right panel), the two together accounting for ~45% of the by-role total; the constraining roles that bind observation to model state – Assimilation (23) and Calibration (11) – are markedly thinner.

Regarding the row axis, the densest aspect is the drivers of changes in erosion and sediment discharge (EA1), with row totals of 57 and 60 in the by-product and by-role pivots respectively, followed by the coupling, calibration and validation aspect (EA7) at 42 and 44. It is noted that EA7, although not the densest row overall, is the densest of the integration aspects and is the one to which the present framework is most directly addressed; the proximity of the two leading rows is consistent with the watershed sediment-discharge drivers and the coupling itself being the twin foci of an integrated Watershed-Coast System approach.

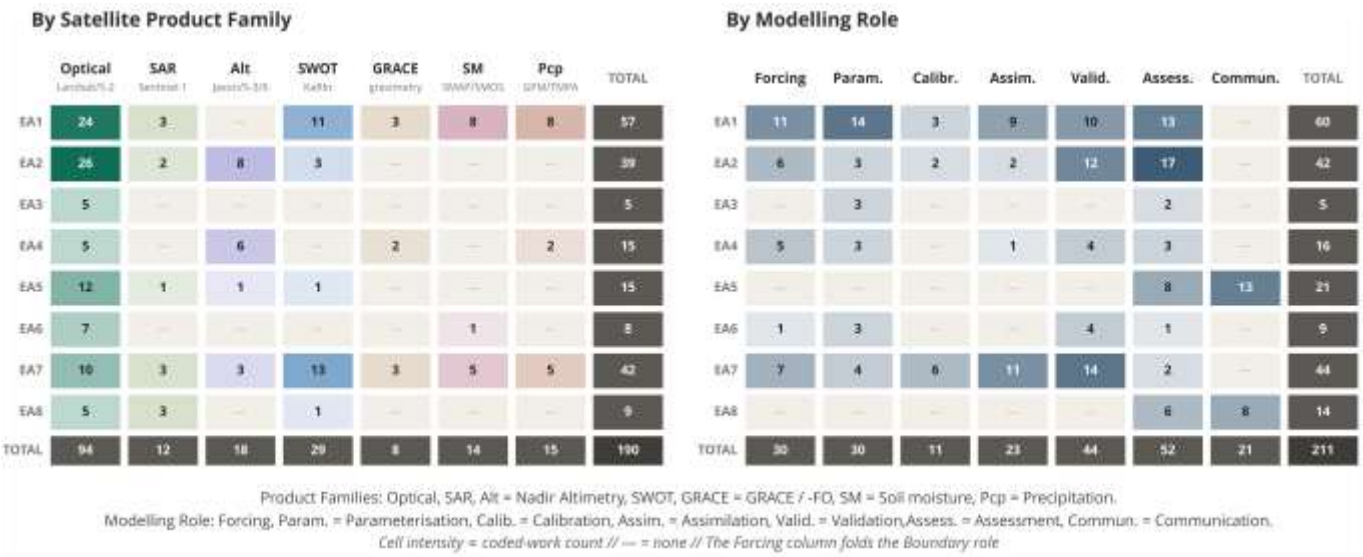


Figure 5. Heatmap composite of coded-work counts by product family (left) and by modelling role (right); official pivots 190 / 211; neutral-grey totals; dash for empty cells. EA1–EA8 are defined in Table 1.

The coupling signature of the framework is read most clearly in the SWOT column. Figure 3 shows that SWOT concentrates in three rows – the drivers of erosion and sediment discharge (EA1), the drivers of coastal morphology (EA2) and the coupling, calibration and validation aspect (EA7) – and that in EA1 and EA7 it spans the full sequence of roles from boundary and forcing through assimilation to validation and assessment (*F:b · C · A · V · As*). This is the fingerprint of a mission that observes the landward and seaward water surfaces in a single swath: as set out in Section 3.4, SWOT supplies the river-mouth discharge boundary on the watershed side (EA1) and the sea-surface elevation on the coastal side (EA2), and it is consumed by the coupling itself (EA7) as both an assimilated state variable and a validation reference. Accordingly, SWOT is the technological centrepiece of the integration argument advanced in this work: it is the one family whose by-product cells span the watershed–coast handover that defines the transitional zone, and its 13 contributions to EA7 (Fig. 5) are the largest single concentration of any family in that aspect.

Regarding the coupling aspect, a worked reading of the EA7 row demonstrates how the two views are used together. In the by-role view (Fig. 4), the Calibration cell for EA7 carries five families (*Opt · Alt · SWOT · SM · Pcp*), the Assimilation cell carries five (*SAR · SWOT · GRACE · SM · Pcp*) and the Validation cell carries six (*Opt · Alt · SWOT · GRACE · SM · Pcp*) – the broadest family span of any cell in the matrix, and the concrete expression of EA7 being the integration aspect. The same row read in the by-product view (Fig. 3) shows the division of labour between families as follows. The optical record acts across boundary, parameterisation, calibration, validation and assessment at the local-to-coastal scale (*F:b · P · C · V · As / L · I*), whereas SWOT acts as boundary, calibrant, assimilant, validation and assessment at the regional scale (*F:b · C · A · V · As / R · D*), and the water-budget families (i.e. gravimetry and soil moisture) enter only through assimilation and validation. The latter pattern is the matrix making explicit what Section 4.1 develops in prose: the coupling is constrained less by any single sensor than by the joint availability of complementary families in the calibration, assimilation and validation roles. The assimilation and calibration works that operationalise this coupling are supplied by Sections 3.2–3.4 and developed in Section 4.1 and are not re-narrated here; the framework records only their placement.

Figure 6 shows the availability of each product family across the spatial and temporal scales, the circle area scaling with the number of coded works and the column margin carrying the full-corpus scale totals. Regarding the spatial dimension, the corpus is weighted towards the regional scale (56 of 119 coded rows), with the local-to-coastal (35) and global (28) scales less represented, and the optical family supplies the bulk of the local-to-

coastal record that the Watershed-Coast System most requires (Fig. 6, left panel). Regarding the temporal dimension, the record is overwhelmingly interannual-to-decadal (74 rows) and daily-to-monthly (42), with the sub-daily band all but absent: only three coded rows across the entire corpus resolve processes finer than one day (Fig. 6, right panel). It is noteworthy, though, that this near-absence of the sub-daily band is a structural limitation of the present satellite record rather than of the coding, since the event- and tidal-scale processes that govern the river-mouth exchange (e.g. storm surge, tidal pump, flood pulse) fall precisely in the band that the polar-orbiting families revisit least often. Nevertheless, the precipitation constellations are the one family with a sub-daily presence, consistent with the sub-daily multi-satellite retrievals characterised for Component (A) in Section 3.1.



Figure 6. Tools across scales: product family × spatial scale and product family × temporal scale; circle area proportional to coded-work count; full-corpus scale marginals shown.

All in all, a particularly informative feature of the framework is not where the literature concentrates, but where it is absent. Figure 3 and Figure 4 show that ~45% of the by-product cells and ~41% of the by-role cells are empty, and these empty cells are not randomly scattered. The Communication role is confined entirely to the two implication aspects, EA5 and EA8 (Fig. 5, right panel), so that the stakeholder-facing use of satellite data developed in Section 4.3 has no presence in the analytical aspects at all. The Calibration and Assimilation roles are thin across every aspect except the coupling aspect EA7; and whole families are absent from the management-and-engineering and seasonality aspects. It is noted that this gap structure is itself a contribution: it identifies, for an integrated Watershed-Coast System approach, exactly which observation–role–aspect combinations remain to be demonstrated, namely: the sub-daily forcing of the transitional zone, the assimilation of satellite-observed morphology into coupled models beyond EA7, and the systematic placement of the off-family sensors.

Regarding those off-family sensors, twelve works carrying non-Sentinel-1 SAR (ENVISAT, TerraSAR-X, RADARSAT-1), ICESat-2 photon altimetry, legacy or coarse sensors (IRS, DMSP SSM/I, MODIS used as an indicator) and generic Earth-observation products are coded and remain visible in the by-role pivot but fall outside the seven by-product families. Accordingly, they are footnoted in Figures 4 and 6 rather than given a column of their own, since each is a one-off demonstration rather than an established family, and the seven-family axis is retained. The full per-work detail behind every cell of the framework – the individual works, their

methods and tools, their modelling roles and their scale assignments – will be provided in an interactive supplement to the published version of this article, which renders both views of the matrix and allows it to be filtered by family, role and aspect and the gap cells to be inspected directly. Beyond the matrix, the same supplement provides a faceted corpus browser over the coded works and a clickable system map of the Watershed-Coast System, so that the evidence can be navigated by individual work and by component as well as by cell.

6. Discussion and the path forward

The discussion advanced in this Section reads the structured framework of Section 5 back against the reviewed literature and against the WACS framework of Samaras (2023), in order to establish where the satellite-modelling evidence concentrates, where it is absent, and what the resulting gap structure implies for an integrated approach to Watershed-Coast System morphodynamics. The per-study details are supplied by Sections 3 and 4 and are not repeated here; the unit of discussion is the framework as a whole.

Figure 5 shows the density of the corpus across the two pivots of the framework, and the first feature it makes plain is the dominance of the optical record. With 94 of the 190 by-product contributions, optical imagery is the single most-used family by a wide margin and is the only family present in all eight essential aspects, a reach consistent with its long-term service across the watershed, the coast and the transitional zone in Sections 3.2–3.4. The Surface Water and Ocean Topography (SWOT) mission is the second most represented family at 29 contributions – a notable position for a mission launched only in late 2022 – while the remaining families occupy more specialised niches, from Nadir Altimetry (18) and the Precipitation constellations (15) to Soil Moisture (14), Synthetic-Aperture Radar (12) and GRACE / gravimetry (8). It is noted that this distribution mirrors the maturity asymmetry identified in the Introduction: the families that serve the well-established watershed and coastal literatures are the densest, and the integration-specific record is carried disproportionately by the one mission designed to bridge the two.

Regarding the modelling roles, Figure 5 shows a corpus weighted towards the downstream and the diagnostic. The Assessment role is the most populated at 52 contributions and Validation follows at 44, the two together accounting for ~45% of the by-role total of 211, whereas the constraining roles that bind an observation to the evolving model state – Assimilation (23) and Calibration (11) – are markedly thinner. Accordingly, the satellite record is most often used to read a modelled or observed result and to check it independently, and least often to drive the model state forward; the integration mechanisms developed in Section 4.1 are, on the evidence of the framework, the least densely populated and therefore the least mature part of the chain.

Figure 3 shows the coupling signature of the framework most clearly in the SWOT column, which concentrates in three rows – the drivers of erosion and sediment discharge (EA1), the drivers of coastal morphology (EA2) and the coupling, calibration and validation aspect (EA7) – and which spans, in EA1 and EA7, the full sequence of roles from boundary and forcing through assimilation to validation and assessment. This is the fingerprint of a mission that observes the landward and seaward water surfaces in a single swath, and its 13 contributions to EA7 (Fig. 5) are the largest single concentration of any family in that aspect. Regarding the row axis, it is noted that the densest row of the framework is not the coupling aspect but EA1, the drivers of erosion and sediment discharge, with row totals of 57 and 60 in the by-product and by-role pivots. The coupling aspect EA7 is the second densest overall (42 and 44) and the densest of the integration aspects. Nevertheless, the proximity of the two leading rows is itself a result: the watershed sediment-discharge drivers and the coupling that consumes them are the twin focal points of an integrated Watershed-Coast System approach, and the satellite

record is now densest precisely where Samaras (2023) located both the essence and the principal difficulty of the concept.

Figure 6 shows the availability of each family across the spatial and temporal scales, and it qualifies the optimism of the coupling signature in two ways. Regarding the spatial dimension, the corpus is weighted towards the regional scale (56 of 119 coded rows), with the local-to-coastal scale (35) – the scale that an integrated Watershed-Coast System approach most requires – carried largely by the optical family. Regarding the temporal dimension, the record is overwhelmingly interannual-to-decadal (74 rows) and daily-to-monthly (42), and only three coded rows across the entire corpus resolve processes finer than one day. It is noteworthy, though, that this near-absence of the sub-daily band is a structural property of the polar-orbiting record rather than an artefact of the coding: the exchange that moves water and sediment across the river mouth on event and tidal timescales is concentrated in exactly the band that these families revisit least, so that the processes most diagnostic of the coupling remain the least observed. This is a limitation that, hopefully, the wide-swath and geostationary record will begin to relax.

All in all, the most consequential reading of the framework is the one Section 5 has already set out: its particularly informative feature is where the literature is absent, not where it is abundant. Those empty cells – the Communication role missing from the analytical aspects, and the Calibration and Assimilation roles thin everywhere but the coupling aspect EA7 – are not a description but a research agenda. The single most consequential of them, foreshadowed in Section 4.1, is the satellite-data-enabled sediment-flux coupling: the river-mouth suspended-sediment flux that closes the watershed-to-coast handover is now well observed, yet it is seldom assimilated into (or used to calibrate) a coupled morphodynamic model. Accordingly, the empty cells define the agenda directly: the sub-daily forcing of the transitional zone, the assimilation of satellite-observed morphology and sediment flux into coupled models beyond EA7, and the systematic placement of the off-family sensors that the seven-family axis presently footnotes. These empty and thin cells will be open to interrogation in the interactive supplement (see Data availability), whose gap view isolates the unpopulated intersections of essential aspect, satellite-product family and modelling role and, for each, lists the neighbouring coded works that mark the current frontier.

Regarding the means by which this agenda becomes tractable, the SWOT-era opening is reinforced by a parallel maturation of cloud-based and machine-learning processing. The automated extraction of shorelines from multi-decadal optical archives, the machine- and deep-learning retrieval of nearshore bathymetry, and the cloud-platform processing of land-cover-change records reviewed by Gu and Zeng (2024) have each narrowed the distance between the raw satellite record and a model-ready product, as developed in Sections 3.2, 3.3 and 4.3. Accordingly, it is the conjunction of a mission that observes the coupling and a processing chain that renders the observation usable that distinguishes the present moment from the one in which the coupling was first identified as the data-poorest link in the chain.

The framework advances the path-to-decision-making of Samaras (2023) by making its essential aspects countable, and it can be read directly against the challenges set out in Table 2 of that work. Where Samaras (2023) identified the integration of the system as the least-studied component, the matrix shows quantitatively which observation–role–aspect combinations have been demonstrated and which remain empty, on a common axis with the analytical and the implication aspects. Regarding the modelling-approach challenges in particular, the framework supplies an observational status for each, as laid out in the following. Regarding the coupling, calibration and validation of Component (D) – rated of high difficulty and promising status – this is borne out by EA7 emerging as the densest integration aspect, yet the persistent thinness of the Calibration and Assimilation roles shows that the promise is not yet realised in the binding mechanisms. Regarding the

challenge of defining quantitative links between the watershed and the coastal processes, this maps precisely to the sediment-flux coupling gap, the river-mouth flux being well observed but seldom assimilated. Regarding the challenge of applicability to management-relevant scales, this is qualified by the regional weighting and the near-absent sub-daily band. And, finally, regarding the challenge of adaptability to ecological and socio-economic implications and to stakeholder engagement – rated at an early stage – this is mirrored in the Communication role being confined to EA5 and EA8.

Regarding the parallel frameworks, the result sits beside rather than against them: the Watershed-Coast Continuum review of Malara et al. (2020) reaches the holistic-monitoring imperative without satellite data, and the Catchment-Estuary-Coastal modelling of Bamunawala et al. (2020) couples the system at reduced complexity from the modelling side, whereas the present framework supplies the observational counterpart that both imply. It is noted, finally, that the gap structure carries a Society-and-Governance reading as well: the same gap between *user-inspired* and *user-ready* provision that recurs across the communication mechanisms of Section 4.3 is the institutional analogue of the empty Communication cells, and the promise of satellite assessment is greatest, as Sheffield et al. (2018) and Beveridge et al. (2020) show, in exactly the data-poor regions where the in situ record is weakest.

7. Conclusions

This work has reviewed the use of satellite data across the four components of the Watershed-Coast System framework of Samaras (2023) and the Science–Society–Governance dimension that bridges them, and has proposed a structured framework that places every coded work at the intersection of an essential aspect, a satellite-product family and a modelling role, qualified by its spatial and temporal scale. The two complementary views of the framework (Figures 3 and 4) resolve the same coded corpus of 113 works into a by-product and a by-role pivot, and its density and scale composites (Figures 5 and 6) reveal a literature that is dense where the watershed and coastal sciences are mature, that concentrates its integration-specific evidence in the coupling aspect EA7, and that is structurally empty in the sub-daily band and across the constraining assimilation and calibration roles.

Regarding the integration argument, the Surface Water and Ocean Topography mission emerges as its technological centrepiece. It is the one family whose framework cells span the watershed–coast handover that defines the transitional zone, and its concentration in the coupling aspect is the largest of any family; the SWOT-era opening, reinforced by cloud-based and machine-learning processing, is the principal reason that the transitional zone (the data-poorest link in the chain for long) is becoming the one most directly served by the satellite observing system.

The framework is intended to be read differently by the three audiences it addresses. For the modeller, it identifies the observation–role–aspect combinations that remain to be demonstrated, and in particular the assimilation of satellite-observed morphology and river-mouth sediment flux into coupled morphodynamic models. For the manager, it locates the scales – regional and, increasingly, local-to-coastal – at which the satellite record can substitute for the in situ networks that the transitional zone systematically lacks. For the policymaker, it makes explicit that the value of the satellite record is realised not by the observation alone but by its translation into a *user-ready*, stakeholder-facing artifact, a translation that the empty Communication cells of the analytical aspects show to be the least developed.

These conclusions are open to a few limitations that have to do with its nature and essence. First, the corpus is frozen and finite, and the framework records the literature as coded rather than the full universe of satellite-

modelling studies. Second, the near-absence of the sub-daily band is a property of the present observing system and may relax as wide-swath and geostationary capabilities mature. And third, the off-family sensors – non-Sentinel-1 synthetic-aperture radar, photon-counting altimetry and legacy or generic products – are heterogeneous one-off demonstrations whose placement on a seven-family axis remains a footnote rather than a column.

Nevertheless, the central conclusion of this work is that the structural integration of satellite data into Watershed-Coast System modelling is, in the SWOT era, no longer constrained chiefly by the observation but by the modelling chain that consumes it. The empty cells of the framework are, accordingly, less a record of what cannot be observed than a research agenda for what has yet to be coupled.

CRediT authorship contribution statement

Achilleas G. Samaras: Conceptualization, Methodology, Investigation, Data curation, Writing – original draft, Writing – review & editing. **Michael Nones:** Conceptualization, Methodology, Investigation, Data curation, Writing – original draft, Writing – review & editing. Both authors contributed equally to this work.

Funding

This research did not receive any specific grant from funding agencies in the public, commercial, or not-for-profit sectors. The work of Michael Nones was partially supported by a subsidy from the Polish Ministry of Education and Science for the Institute of Geophysics, Polish Academy of Sciences.

Data availability

The data that support the framework presented in this work – the coded corpus of 113 works with their component, sub-domain, method, tool, modelling-role, spatial- and temporal-scale and essential-aspect assignments – will be released as an interactive HTML supplement with the published version of this article. Until then, the corpus and its full bibliographic list are available from the corresponding author on reasonable request. No separate data-repository deposit is associated with this study.

Declaration of generative AI and AI-assisted technologies

During the preparation of this work, the authors used Claude (Anthropic) to proofread and improve the English language of the manuscript. The authors reviewed and edited the output as needed and take full responsibility for the content of the published article.

References

Ablain, M., Legeais, J.F., Prandi, P., Marcos, M., Fenoglio-Marc, L., Dieng, H.B., Benveniste, J., Cazenave, A., 2017. Satellite Altimetry-Based Sea Level at Global and Regional Scales. Surv Geophys 38 (1), 7-31. https://doi.org/10.1007/s10712-016-9389-8

Agnoli, L., Urquhart, E., Georgantzis, N., Schaeffer, B., Simmons, R., Hoque, B., Neely, M.B., Neil, C., Oliver, J., Tyler, A., 2023. Perspectives on user engagement of satellite Earth observation for water quality management. Technological Forecasting and Social Change 189, 122357. https://doi.org/10.1016/j.techfore.2023.122357

Amarouche, K., Akpınar, A., Soran, M.B., Myslenkov, S., Majidi, A.G., Kankal, M., Arkhipkin, V., 2021. Spatial calibration of an unstructured SWAN model forced with CFSR and ERA5 winds for the Black and Azov Seas. Applied Ocean Research 117, 102962. https://doi.org/10.1016/j.apor.2021.102962

Andreadis, K.M., Coss, S.P., Durand, M., Gleason, C.J., Simmons, T.T., Tebaldi, N., Bjerklie, D.M., Brinkerhoff, C., Dudley, R.W., Gejadze, I., Larnier, K., Malaterre, P.O., Oubanas, H., Allen, G.H., Bates, P.D., David, C.H., Domeneghetti, A., Elmi, O., Marc, L.F., Prata de Moraes Frasson, R., Friedmann, E., Garambois, P.A., Gehring, J., Getirana, A., Hughes, M., Lee, J., Matte, P., Minear, J.T., Monnier, J., Muhebwa, A., Tourian, M.J., Pavelsky, T.M., Riggs, R.M., Rodríguez, E., Sikder, M.S., Smith, L.C., Stuurman, C., Taneja, J., Tarpanelli, A., Wang, J., Williams, B.A., Yadav, B., 2025. A First Look at River Discharge Estimation From SWOT Satellite Observations. Geophysical Research Letters 52 (9). https://doi.org/10.1029/2024gl114185

Andriolo, U., Almeida, L.P., Almar, R., 2018. Coupling terrestrial LiDAR and video imagery to perform 3D intertidal beach topography. Coastal Engineering 140, 232-239. https://doi.org/10.1016/j.coastaleng.2018.07.009
Ashphaq, M., Srivastava, P.K., Mitra, D., 2024. Satellite-Derived Bathymetry in Dynamic Coastal Geomorphological Environments Through Machine Learning Algorithms. Earth and Space Science 11 (7). https://doi.org/10.1029/2024ea003554
Bamunawala, J., Dastgheib, A., Ranasinghe, R., van der Spek, A., Maskey, S., Murray, A.B., Duong, T.M., Barnard, P.L., Sirisena, T.A.J.G., 2020. A Holistic Modeling Approach to Project the Evolution of Inlet-Interrupted Coastlines Over the 21st Century. Front. Mar. Sci. 7. https://doi.org/10.3389/fmars.2020.00542
Beck, H.E., Vergopolan, N., Pan, M., Levizzani, V., van Dijk, A.I.J.M., Weedon, G.P., Brocca, L., Pappenberger, F., Huffman, G.J., Wood, E.F., 2017. Global-scale evaluation of 22 precipitation datasets using gauge observations and hydrological modeling. Hydrol. Earth Syst. Sci. 21 (12), 6201-6217. https://doi.org/10.5194/hess-21-6201-2017
Bergsma, E.W.J., Almar, R., Rolland, A., Binet, R., Brodie, K.L., Bak, A.S., 2021. Coastal morphology from space: A showcase of monitoring the topography-bathymetry continuum. Remote Sensing of Environment 261, 112469. https://doi.org/10.1016/j.rse.2021.112469
Beveridge, C., Hossain, F., Biswas, R.K., Haque, A.A., Ahmad, S.K., Biswas, N.K., Hossain, M.A., Bhuyan, M.A., 2020. Stakeholder-driven development of a cloud-based, satellite remote sensing tool to monitor suspended sediment concentrations in major Bangladesh rivers. Environmental Modelling & Software 133, 104843. https://doi.org/10.1016/j.envsoft.2020.104843
Bhaskar, A.S., Kumar, R.B.B., 2011. Remote sensing of coastal geomorphology to understand river migration in the Thengapatnam area, southern India. International Journal of Remote Sensing 32 (18), 5287-5301. https://doi.org/10.1080/01431161.2010.497509
Bhattarai, T.N., Moreno-Rodenas, A., Giri, S., Bakker, M., Omer, A., Bateman, A., 2026. Quantifying river morphological changes using multi-satellite observations and in situ measurements. Earth Surf Processes Landf 51 (3). https://doi.org/10.1002/esp.70263
Biancamaria, S., Lettenmaier, D.P., Pavelsky, T.M., 2016. The SWOT Mission and Its Capabilities for Land Hydrology. Surv Geophys 37 (2), 307-337. https://doi.org/10.1007/s10712-015-9346-y
Busch, J.A., Price, I., Jeansou, E., Zielinski, O., van der Woerd, H.J., 2016. Citizens and satellites: Assessment of phytoplankton dynamics in a NW Mediterranean aquaculture zone. International Journal of Applied Earth Observation and Geoinformation 47, 40-49. https://doi.org/10.1016/j.jag.2015.11.017
Caballero, I., Stumpf, R.P., 2019. Retrieval of nearshore bathymetry from Sentinel-2A and 2B satellites in South Florida coastal waters. Estuarine, Coastal and Shelf Science 226, 106277. https://doi.org/10.1016/j.ecss.2019.106277
Cabezas-Rabadán, C., Pardo-Pascual, J.E., Palomar-Vázquez, J., Fernández-Sarría, A., 2019. Characterizing beach changes using high-frequency Sentinel-2 derived shorelines on the Valencian coast (Spanish Mediterranean). Science of The Total Environment 691, 216-231. https://doi.org/10.1016/j.scitotenv.2019.07.084
Capo, S., Lubac, B., Marieu, V., Robinet, A., Bru, D., Bonneton, P., 2014. Assessment of the decadal morphodynamic evolution of a mixed energy inlet using ocean color remote sensing. Ocean Dynamics 64 (10), 1517-1530. https://doi.org/10.1007/s10236-014-0762-1
Caracciolo, D., Francipane, A., Viola, F., Noto, L.V., Deidda, R., 2018. Performances of GPM satellite precipitation over the two major Mediterranean islands. Atmospheric Research 213, 309-322. https://doi.org/10.1016/j.atmosres.2018.06.010
Carvalho, B.C., Dalbosco, A.L.P., Guerra, J.V., 2020. Shoreline position change and the relationship to annual and interannual meteo-oceanographic conditions in Southeastern Brazil. Estuarine, Coastal and Shelf Science 235, 106582. https://doi.org/10.1016/j.ecss.2020.106582
Cenci, L., Disperati, L., Persichillo, M.G., Oliveira, E.R., Alves, F.L., Phillips, M., 2017. Integrating remote sensing and GIS techniques for monitoring and modeling shoreline evolution to support coastal risk management. GIScience & Remote Sensing 55 (3), 355-375. https://doi.org/10.1080/15481603.2017.1376370
Cerbaro, M., Morse, S., Murphy, R., Lynch, J., Griffiths, G., 2020. Information from Earth Observation for the Management of Sustainable Land Use and Land Cover in Brazil: An Analysis of User Needs. Sustainability 12 (2), 489. https://doi.org/10.3390/su12020489
Cerbelaud, A., David, C.H., Pavelsky, T., Biancamaria, S., Garambois, P.A., Kittel, C., Papa, F., Bates, P., Tourian, M.J., Durand, M., Frasson, R., Oubanas, H., Simard, M., Schumann, G., Allen, G., Tarpanelli, A., Wongchuig, S., Wade, J., Tom, M., Malaterre, P.O., Gleason, C.J., Crétaux, J.F., Nielsen, K., Elmi, O., Schwatke, C., Scherer, D., Gal, L., Paris, A., Dasgupta, A., Munier, S., Feng, D., Bauer-Gottwein, P., Hossain, F., Yamazaki, D., Kitambo, B., Mischel, S., Bonnema, M., Verma, K., Andreadis, K., Picot, N., Benveniste, J., 2025. Satellite Requirements to Capture Water Propagation in Earth's Rivers. Reviews of Geophysics 63 (3). https://doi.org/10.1029/2024rg000871
Chakrabortty, R., Pradhan, B., Mondal, P., Pal, S.C., 2020. The use of RUSLE and GCMs to predict potential soil erosion associated with climate change in a monsoon-dominated region of eastern India. Arab J Geosci 13 (20). https://doi.org/10.1007/s12517-020-06033-y

Chang, C.-H., Lee, H., Kim, D., Hwang, E., Hossain, F., Chishtie, F., Jayasinghe, S., Basnayake, S., 2020. Hindcast and forecast of daily inundation extents using satellite SAR and altimetry data with rotated empirical orthogonal function analysis: Case study in Tonle Sap Lake Floodplain. Remote Sensing of Environment 241, 111732. https://doi.org/10.1016/j.rse.2020.111732
Chao, L., Zhang, K., Yang, Z.-L., Wang, J., Lin, P., Liang, J., Li, Z., Gu, Z., 2021. Improving flood simulation capability of the WRF-Hydro-RAPID model using a multi-source precipitation merging method. Journal of Hydrology 592, 125814. https://doi.org/10.1016/j.jhydrol.2020.125814
Charoensuk, T., Luchner, J., Bauer-Gottwein, P., 2025. Leveraging Ice, Cloud, and Land Elevation Satellite-2 Laser Altimetry and Surface Water Ocean Topography Radar Altimetry for Error Diagnosis in Hydraulic Models: A Case Study of the Chao Phraya River. Remote Sensing 17 (4), 621. https://doi.org/10.3390/rs17040621
Chen, F., Crow, W.T., Starks, P.J., Moriasi, D.N., 2011. Improving hydrologic predictions of a catchment model via assimilation of surface soil moisture. Advances in Water Resources 34 (4), 526-536. https://doi.org/10.1016/j.advwatres.2011.01.011
Chen, F., Crow, W.T., Bindlish, R., Colliander, A., Burgin, M.S., Asanuma, J., Aida, K., 2018. Global-scale evaluation of SMAP, SMOS and ASCAT soil moisture products using triple collocation. Remote Sensing of Environment 214, 1-13. https://doi.org/10.1016/j.rse.2018.05.008
Clement, S., Jozaei, J., Mitchell, M., Allen, C.R., Garmestani, A.S., 2023. How resilience is framed matters for governance of coastal social-ecological systems. Env Pol Gov 34 (1), 65-76. https://doi.org/10.1002/eet.2056
Crow, W.T., Berg, A.A., Cosh, M.H., Loew, A., Mohanty, B.P., Panciera, R., de Rosnay, P., Ryu, D., Walker, J.P., 2012. Upscaling sparse ground-based soil moisture observations for the validation of coarse-resolution satellite soil moisture products. Reviews of Geophysics 50 (2). https://doi.org/10.1029/2011rg000372
Cui, B.-L., Li, X.-Y., 2011. Coastline change of the Yellow River estuary and its response to the sediment and runoff (1976–2005). Geomorphology 127 (1-2), 32-40. https://doi.org/10.1016/j.geomorph.2010.12.001
De Leeuw, J., Georgiadou, Y., Kerle, N., De Gier, A., Inoue, Y., Ferwerda, J., Smies, M., Narantuya, D., 2010. The Function of Remote Sensing in Support of Environmental Policy. Remote Sensing 2 (7), 1731-1750. https://doi.org/10.3390/rs2071731
Duan, L., Man, X., Kurylyk, B.L., Cai, T., Li, Q., 2017. Distinguishing streamflow trends caused by changes in climate, forest cover, and permafrost in a large watershed in northeastern China. Hydrological Processes 31 (10), 1938-1951. https://doi.org/10.1002/hyp.11160
Eini, M.R., Massari, C., Piniewski, M.A., 2023. Satellite-based soil moisture enhances the reliability of agro-hydrological modeling in large transboundary river basins. Science of The Total Environment 873, 162396. https://doi.org/10.1016/j.scitotenv.2023.162396
Entekhabi, D., Njoku, E.G., O'Neill, P.E., Kellogg, K.H., Crow, W.T., Edelstein, W.N., Entin, J.K., Goodman, S.D., Jackson, T.J., Johnson, J., Kimball, J., Piepmeier, J.R., Koster, R.D., Martin, N., McDonald, K.C., Moghaddam, M., Moran, S., Reichle, R., Shi, J.C., Spencer, M.W., Thurman, S.W., Tsang, L., Van Zyl, J., 2010. The Soil Moisture Active Passive (SMAP) Mission. Proc. IEEE 98 (5), 704-716. https://doi.org/10.1109/jproc.2010.2043918
Filippi, E., Aiello, A., 2025. Enablers and Barriers to EO Satellite Data Uptake in European Local Authorities. Urban Science 9 (11), 489. https://doi.org/10.3390/urbansci9110489
Fu, Y., Wu, Q., 2024. Recent Emerging Shifts in Precipitation Intensity and Frequency in the Global Tropics Observed by Satellite Precipitation Data Sets. Geophysical Research Letters 51 (15). https://doi.org/10.1029/2023gl107916
Gensac, E., Martinez, J.-M., Vantrepotte, V., Anthony, E.J., 2016. Seasonal and inter-annual dynamics of suspended sediment at the mouth of the Amazon river: The role of continental and oceanic forcing, and implications for coastal geomorphology and mud bank formation. Continental Shelf Research 118, 49-62. https://doi.org/10.1016/j.csr.2016.02.009
George, C.F., Macdonald, D.I.M., Spagnolo, M., 2019. Deltaic sedimentary environments in the Niger Delta, Nigeria. Journal of African Earth Sciences 160, 103592. https://doi.org/10.1016/j.jafrearsci.2019.103592
Gleason, C.J., Hamdan, A.N., 2015. Crossing the (watershed) divide: satellite data and the changing politics of international river basins. Geographical Journal 183 (1), 2-15. https://doi.org/10.1111/geoj.12155
Gomes da Silva, P., Jara, M.S., Medina, R., Beck, A.-L., Taji, M.A., 2024. On the use of satellite information to detect coastal change: Demonstration case on the coast of Spain. Coastal Engineering 191, 104517. https://doi.org/10.1016/j.coastaleng.2024.104517
Gómez, C., Wulder, M.A., Dawson, A.G., Ritchie, W., Green, D.R., 2014. Shoreline Change and Coastal Vulnerability Characterization with Landsat Imagery: A Case Study in the Outer Hebrides, Scotland. Scottish Geographical Journal 130 (4), 279-299. https://doi.org/10.1080/14702541.2014.923579
Gómez, J.F., Kwoll, E., Walker, I.J., Shirzaei, M., 2021. Vertical Land Motion as a Driver of Coastline Changes on a Deltaic System in the Colombian Caribbean. Geosciences 11 (7), 300. https://doi.org/10.3390/geosciences11070300
Gosnell, H., Kennedy, R., Harris, T., Abrams, J., 2020. A land systems science approach to assessing forest governance and characterizing the emergence of social forestry in the Western Cascades of Oregon. Environ. Res. Lett. 15 (5), 055003. https://doi.org/10.1088/1748-9326/ab666b
Gu, Z., Zeng, M., 2024. The Use of Artificial Intelligence and Satellite Remote Sensing in Land Cover Change Detection: Review and Perspectives. Sustainability 16 (1), 274. https://doi.org/10.3390/su16010274

Gupta, S., Kumar, S., 2017. Simulating climate change impact on soil erosion using RUSLE model − A case study in a watershed of mid-Himalayan landscape. J Earth Syst Sci 126 (3). https://doi.org/10.1007/s12040-017-0823-1
Hassan, M.I., Rahmat, N.H., 2016. THE EFFECT OF COASTLINE CHANGES TO LOCAL COMMUNITY'S SOCIAL-ECONOMIC. Int. Arch. Photogramm. Remote Sens. Spatial Inf. Sci. XLII-4/W1, 25-36. https://doi.org/10.5194/isprs-archives-xlii-4-w1-25-2016
Heerma van Voss, B., Ouellette, W., 2024. Granular satellite data to assess the potential for nature based solutions at a national scale: a proof of concept with data from Rwanda and Lesotho. Climate Policy 24 (8), 1112-1128. https://doi.org/10.1080/14693062.2024.2330373
Hostache, R., Chini, M., Giustarini, L., Neal, J., Kavetski, D., Wood, M., Corato, G., Pelich, R.M., Matgen, P., 2018. Near-Real-Time Assimilation of SAR-Derived Flood Maps for Improving Flood Forecasts. Water Resources Research 54 (8), 5516-5535. https://doi.org/10.1029/2017wr022205
Hou, X., Xie, D., Feng, L., Shen, F., Nienhuis, J.H., 2024. Sustained increase in suspended sediments near global river deltas over the past two decades. Nat Commun 15 (1). https://doi.org/10.1038/s41467-024-47598-6
Huffman, G.J., Bolvin, D.T., Nelkin, E.J., Wolff, D.B., Adler, R.F., Gu, G., Hong, Y., Bowman, K.P., Stocker, E.F., 2007. The TRMM Multisatellite Precipitation Analysis (TMPA): Quasi-Global, Multiyear, Combined-Sensor Precipitation Estimates at Fine Scales. Journal of Hydrometeorology 8 (1), 38-55. https://doi.org/10.1175/jhm560.1
Ishikawa, Y., Yamazaki, D., Yang, Y., 2025. Evaluation of a Width-Based Satellite Discharge Algorithm for Detecting Longitudinal Flow Changes in a Human-Regulated Continental River Basin. Geophysical Research Letters 52 (18). https://doi.org/10.1029/2024gl114191
Izaguirre, C., Mendez, F.J., Menendez, M., Luceño, A., Losada, I.J., 2010. Extreme wave climate variability in southern Europe using satellite data. J. Geophys. Res. 115 (C4). https://doi.org/10.1029/2009jc005802
Izaguirre, C., Méndez, F.J., Menéndez, M., Losada, I.J., 2011. Global extreme wave height variability based on satellite data. Geophysical Research Letters, 38 (10). https://doi.org/10.1029/2011GL047302
Jamali, A., Ramazani, M.E., Nejaei, A., Rafieyan, O., 2025. Monitoring of Pollutants in Surface Water with Laboratory Analysis and Satellite Image Between 2019 and 2024, Kichik Chai River, Iran. Water Air Soil Pollut 236 (5). https://doi.org/10.1007/s11270-025-07808-3
Janušaitė, R., Jukna, L., Jarmalavičius, D., Pupienis, D., Žilinskas, G., 2021. A Novel GIS-Based Approach for Automated Detection of Nearshore Sandbar Morphological Characteristics in Optical Satellite Imagery. Remote Sensing 13 (11), 2233. https://doi.org/10.3390/rs13112233
Jia, Y., Liu, Q., Song, C., Xiao, Z., Dai, Q., Jin, S., Savi, P., 2025. Fusing SAR image and CYGNSS data for monitoring river water level changes by machine learning. Remote Sensing of Environment 329, 114927. https://doi.org/10.1016/j.rse.2025.114927
Jiang, L., Bauer-Gottwein, P., 2019. How do GPM IMERG precipitation estimates perform as hydrological model forcing? Evaluation for 300 catchments across Mainland China. Journal of Hydrology 572, 486-500. https://doi.org/10.1016/j.jhydrol.2019.03.042
Jimenez, J., Tripathi, N., Pandey, A., Shrestha, S., Chao, K., Gatela Jr., E., Jimenez Jr., J., Aspiras, J., 2025. Geospatial Governance for Sustainable Water Resources Management: Integrating SWAT Modeling, Satellite Data, and Hydrogeological Units in Padsan River Watershed. International Journal of Geoinformatics, 21 (10), 4525. https://doi.org/10.52939/ijg.v21i10.4525
Kong, D., Latrubesse, E.M., Miao, C., Zhou, R., 2020. Morphological response of the Lower Yellow River to the operation of Xiaolangdi Dam, China. Geomorphology 350, 106931. https://doi.org/10.1016/j.geomorph.2019.106931
Laignel, B., Vignudelli, S., Almar, R., Becker, M., Bentamy, A., Benveniste, J., Birol, F., Frappart, F., Idier, D., Salameh, E., Passaro, M., Menende, M., Simard, M., Turki, E.I., Verpoorter, C., 2023. Observation of the Coastal Areas, Estuaries and Deltas from Space. Surveys in Geophysics, 44 (5), pp.1309-1356. https://doi.org/10.1007/s10712-022-09757-6
Lazarus, E.D., Williams, H.E., Goldstein, E.B., 2022. Volume Estimation From Planform Characteristics of Washover Morphology. Geophysical Research Letters 49 (22). https://doi.org/10.1029/2022gl100098
Li, B., Rodell, M., Kumar, S., Beaudoing, H.K., Getirana, A., Zaitchik, B.F., de Goncalves, L.G., Cossetin, C., Bhanja, S., Mukherjee, A., Tian, S., Tangdamrongsub, N., Long, D., Nanteza, J., Lee, J., Policelli, F., Goni, I.B., Daira, D., Bila, M., de Lannoy, G., Mocko, D., Steele-Dunne, S.C., Save, H., Bettadpur, S., 2019. Global GRACE Data Assimilation for Groundwater and Drought Monitoring: Advances and Challenges. Water Resources Research 55 (9), 7564-7586. https://doi.org/10.1029/2018wr024618
Li, P., Wang, G., Liang, C., Wang, H., Li, Z., 2023. InSAR-Derived Coastal Subsidence Reveals New Inundation Scenarios Over the Yellow River Delta. IEEE J. Sel. Top. Appl. Earth Observations Remote Sensing 16, 8431-8441. https://doi.org/10.1109/jstars.2023.3272782
Li, P., Zhang, Y., Liang, C., Wang, H., Li, Z., 2024. High Spatiotemporal Resolution River Networks Mapping on Catchment Scale Using Satellite Remote Sensing Imagery and DEM Data. Geophysical Research Letters 51 (6). https://doi.org/10.1029/2023gl107956
Lichtman, I.D., Bell, P.S., Gommenginger, C., Banks, C., Calafat, F.M., Brown, J., Williams, S.D.P., 2025. Evaluating Water Levels From the Surface Water and Ocean Topography (SWOT) Mission in a Hyper-Tidal Coastal and Estuarine Environment. Earth and Space Science 12 (7). https://doi.org/10.1029/2024ea004104

Lievens, H., Reichle, R.H., Liu, Q., De Lannoy, G.J.M., Dunbar, R.S., Kim, S.B., Das, N.N., Cosh, M., Walker, J.P., Wagner, W., 2017. Joint Sentinel-1 and SMAP data assimilation to improve soil moisture estimates. Geophysical Research Letters 44 (12), 6145-6153. https://doi.org/10.1002/2017gl073904
Lobeto, H., Menendez, M., Losada, I.J., 2018. Toward a Methodology for Estimating Coastal Extreme Sea Levels From Satellite Altimetry. JGR Oceans 123 (11), 8284-8298. https://doi.org/10.1029/2018jc014487
López López, P., Sutanudjaja, E.H., Schellekens, J., Sterk, G., Bierkens, M.F.P., 2017. Calibration of a large-scale hydrological model using satellite-based soil moisture and evapotranspiration products. Hydrol. Earth Syst. Sci. 21 (6), 3125-3144. https://doi.org/10.5194/hess-21-3125-2017
Luan, H.L., Ding, P.X., Wang, Z.B., Ge, J.Z., 2017. Process-based morphodynamic modeling of the Yangtze Estuary at a decadal timescale: Controls on estuarine evolution and future trends. Geomorphology 290, 347-364. https://doi.org/10.1016/j.geomorph.2017.04.016
Luijendijk, A., Hagenaars, G., Ranasinghe, R., Baart, F., Donchyts, G., Aarninkhof, S., 2018. The State of the World's Beaches. Sci Rep 8 (1). https://doi.org/10.1038/s41598-018-24630-6
Ma, J., Wang, J., He, S., Zhang, J., Liu, L., Zhong, X., Wu, F., 2026. Synchronous coupling dominates human–nature interactions in China: Evidence from nine-quadrant trajectory analysis. Ecological Indicators 185, 114757. https://doi.org/10.1016/j.ecolind.2026.114757
Maffei, S., Leoni, F., Villari, B., 2020. Data-driven anticipatory governance. Emerging scenarios in data for policy practices. Policy Design and Practice 3 (2), 123-134. https://doi.org/10.1080/25741292.2020.1763896
Maiti, S., Bhattacharya, A.K., 2011. A three-unit-based approach in coastal-change studies using Landsat images. International Journal of Remote Sensing 32 (1), 209-229. https://doi.org/10.1080/01431160903439965
Malara, G., Zema, D.A., Arena, F., Bombino, G., Zimbone, S.M., 2020. Coupling watershed - coast systems to study evolutionary trends: A review. Earth-Science Reviews 201, 103040. https://doi.org/10.1016/j.earscirev.2019.103040
Marghany, M., 2012. DInSAR technique for three-dimensional coastal spit simulation from radarsat-1 fine mode data. Acta Geophys. 61 (2), 478-493. https://doi.org/10.2478/s11600-012-0061-5
McCarthy, M.J., Colna, K.E., El-Mezayen, M.M., Laureano-Rosario, A.E., Méndez-Lázaro, P., Otis, D.B., Toro-Farmer, G., Vega-Rodriguez, M., Muller-Karger, F.E., 2017. Satellite Remote Sensing for Coastal Management: A Review of Successful Applications. Environmental Management 60 (2), 323-339. https://doi.org/10.1007/s00267-017-0880-x
Mendelsohn, R., Kurukulasuriya, P., Basist, A., Kogan, F., Williams, C., 2007. Climate analysis with satellite versus weather station data. Climatic Change 81 (1), 71-83. https://doi.org/10.1007/s10584-006-9139-x
Mohammad, A.H., Ghanem, M., De La Hera-rica, P.A., Al Rowwad, A.A., Shatanawi, K., 2025. Satellite- based drought indicators for supporting sustainable water management. Global Journal of Environmental Science and Management, 11 (4), 1493-1508. https://doi.org/10.22034/gjesm.2025.04.08
Mohammed, I.N., Bolten, J.D., Srinivasan, R., Lakshmi, V., 2018. Satellite observations and modeling to understand the Lower Mekong River Basin streamflow variability. Journal of Hydrology 564, 559-573. https://doi.org/10.1016/j.jhydrol.2018.07.030
Munasinghe, D., Cohen, S., Gadiraju, K., 2021. A Review of Satellite Remote Sensing Techniques of River Delta Morphology Change. Remote Sens Earth Syst Sci 4 (1-2), 44-75. https://doi.org/10.1007/s41976-021-00044-3
Munier, S., Polebistki, A., Brown, C., Belaud, G., Lettenmaier, D.P., 2015. SWOT data assimilation for operational reservoir management on the upper Niger River Basin. Water Resour. Res. 51 (1), 554-575. https://doi.org/10.1002/2014wr016157
Nandi, D., Tripathy, J.K., Behera, D., Beuria, R., Thakur, R.R., 2026. Advancing watershed science: A comprehensive review of morphometry, land use change, vulnerability, and resilience frameworks. Physics and Chemistry of the Earth, Parts A/B/C 144, 104412. https://doi.org/10.1016/j.pce.2026.104412
Ndour, A., Laïbi, R.A., Sadio, M., Degbe, C.G.E., Diaw, A.T., Oyédé, L.M., Anthony, E.J., Dussouillez, P., Sambou, H., Dièye, E.H.B., 2018. Management strategies for coastal erosion problems in west Africa: Analysis, issues, and constraints drawn from the examples of Senegal and Benin. Ocean & Coastal Management 156, 92-106. https://doi.org/10.1016/j.ocecoaman.2017.09.001
Ngalande, C., Armenakis, C., 2025. Machine and deep learning methods for satellite-derived bathymetric mapping in Canadian coastal waters. Geomatica 77 (2), 100088. https://doi.org/10.1016/j.geomat.2025.100088
Nones, M., Guerrero, M., Schippa, L., Cavalieri, I., 2024. Remote sensing assessment of anthropogenic and climate variation effects on river channel morphology and vegetation: Impact of dry periods on a European piedmont river. Earth Surf Processes Landf 49 (5), 1632-1652. https://doi.org/10.1002/esp.5791
Normandin, C., Frappart, F., Baghdadi, N., Bourrel, L., Peña Luque, S., Ygorra, B., Kitambo, B., Papa, F., Riazanoff, S., Wigneron, J.-P., 2024. First results of the surface water ocean topography (SWOT) observations to rivers elevation profiles in the Cuvette Centrale of the Congo Basin. Front. Remote Sens. 5. https://doi.org/10.3389/frsen.2024.1466695
Ortenzi, S., Massari, C., Ciabatta, L., Cencetti, C., Dionigi, M., Marchesini, I., Stelluti, M., Di Matteo, L., 2025. Leveraging SMAP-Based Soil Moisture to Identify Runoff Thresholds on Flash Flood–Prone Basins in the Mediterranean Region. Journal of Hydrometeorology, 26 (7), 975-990. https://doi.org/10.1175/JHM-D-24-0143.1

Pareta, K., Pareta, U., 2012. Integrated watershed modeling and characterization using GIS and remote sensing techniques. Indian J. Eng. 1 (1), 81-91.
Patidar, G., Paris, A., Indu, J., Karmakar, S., 2025. How can SWOT derived water surface elevations help calibrating a distributed hydrological model?. Journal of Hydrology 656, 132968. https://doi.org/10.1016/j.jhydrol.2025.132968
Pavelsky, T.M., Durand, M.T., Andreadis, K.M., Beighley, R.E., Paiva, R.C.D., Allen, G.H., Miller, Z.F., 2014. Assessing the potential global extent of SWOT river discharge observations. Journal of Hydrology 519, 1516-1525. https://doi.org/10.1016/j.jhydrol.2014.08.044
Payandeh, A.R., Simard, M., Jensen, D., Campbell, A.D., van Deventer, H., Christensen, A., 2026. A fully satellite-driven workflow for hydrodynamic modeling in data-scarce coastal systems: integrating ICESat-2, Sentinel-2, SWOT and reanalysis models. Front. Remote Sens. 7. https://doi.org/10.3389/frsen.2026.1751006
Pignotti, G., Crawford, M., Han, E., Williams, M.R., Chaubey, I., 2023. SMAP soil moisture data assimilation impacts on water quality and crop yield predictions in watershed modeling. Journal of Hydrology 617, 129122. https://doi.org/10.1016/j.jhydrol.2023.129122
Pleskachevsky, A.L., Rosenthal, W., Lehner, S., 2016. Meteo-marine parameters for highly variable environment in coastal regions from satellite radar images. ISPRS Journal of Photogrammetry and Remote Sensing 119, 464-484. https://doi.org/10.1016/j.isprsjprs.2016.02.001
Poirier, C., Hermes, M., Aliberti, M., 2024. The role of space-based data in European climate policies. Acta Astronautica 214, 439-443. https://doi.org/10.1016/j.actaastro.2023.10.029
Quinn, N.W.T., Sridharan, V., Ramirez-Avila, J., Imen, S., Gao, H., Talchabhadel, R., Kumar, S., McDonald, W., 2022. Applications of GIS and remote sensing in public participation and stakeholder engagement for watershed management. SESMO 4, 18149. https://doi.org/10.18174/sesmo.18149
Reguero, B.G., Menéndez, M., Méndez, F.J., Mínguez, R., Losada, I.J., 2012. A Global Ocean Wave (GOW) calibrated reanalysis from 1948 onwards. Coastal Engineering 65, 38-55. https://doi.org/10.1016/j.coastaleng.2012.03.003
Reiners, P., Sobrino, J., Kuenzer, C., 2023. Satellite-Derived Land Surface Temperature Dynamics in the Context of Global Change—A Review. Remote Sensing 15 (7), 1857. https://doi.org/10.3390/rs15071857
Salomons, W., 2005. Sediments in the Catchment-coast Continuum (7 pp). J Soils Sediments 5 (1), 2-8. https://doi.org/10.1065/jss2005.01.129
Samaras, A.G., Koutitas, C.G., 2014a. The impact of watershed management on coastal morphology: A case study using an integrated approach and numerical modeling. Geomorphology 211, 52-63. https://doi.org/10.1016/j.geomorph.2013.12.029
Samaras, A.G., Koutitas, C.G., 2014b. Modeling the impact of climate change on sediment transport and morphology in coupled watershed-coast systems: A case study using an integrated approach. International Journal of Sediment Research 29 (3), 304-315. https://doi.org/10.1016/s1001-6279(14)60046-9
Samaras, A.G., 2023. Towards integrated modelling of Watershed-Coast System morphodynamics in a changing climate: A critical review and the path forward. Science of The Total Environment 882, 163625. https://doi.org/10.1016/j.scitotenv.2023.163625
Santos, C.A.G., Nascimento, T.V.M.D., Mishra, M., Silva, R.M.D., 2021. Analysis of long- and short-term shoreline change dynamics: A study case of João Pessoa city in Brazil. Science of The Total Environment 769, 144889. https://doi.org/10.1016/j.scitotenv.2020.144889
Sheffield, J., Wood, E.F., Pan, M., Beck, H., Coccia, G., Serrat-Capdevila, A., Verbist, K., 2018. Satellite Remote Sensing for Water Resources Management: Potential for Supporting Sustainable Development in Data-Poor Regions. Water Resources Research 54 (12), 9724-9758. https://doi.org/10.1029/2017wr022437
Sufyan, A., Akhwady, R., Purbani, D., Putra, A., Wisha, U.J., Ekawati, K.N., Dody, S., Nova, S., Mahabror, D., Sujantoko, Prarikeslan, W., Muttaqin, A.D., Shofwan, M., 2025. Evolution of the Porong River Estuary, Indonesia: Morphological Changes of Lusi Island through Sediment Modeling and Time-Series Interpretation of MNDWI. Anthropocene Coasts 8 (1). https://doi.org/10.1007/s44218-025-00101-0
Susilowati, Y., Nur, W.H., Sulaiman, A., Kumoro, Y., Yunarto, 2022. Study of dynamics of coastal sediment cell boundary in Cirebon coastal area based on integrated shoreline Montecarlo model and remote sensing data. Regional Studies in Marine Science 52, 102268. https://doi.org/10.1016/j.rsma.2022.102268
Tapley, B.D., Watkins, M.M., Flechtner, F., Reigber, C., Bettadpur, S., Rodell, M., Sasgen, I., Famiglietti, J.S., Landerer, F.W., Chambers, D.P., Reager, J.T., Gardner, A.S., Save, H., Ivins, E.R., Swenson, S.C., Boening, C., Dahle, C., Wiese, D.N., Dobslaw, H., Tamisiea, M.E., Velicogna, I., 2019. Contributions of GRACE to understanding climate change. Nat. Clim. Chang. 9 (5), 358-369. https://doi.org/10.1038/s41558-019-0456-2
Terracciano, S., Montes, J., Brunetta, R., Cabrita, P., Ciavola, P., Armaroli, C., 2026. Influence of Posidonia oceanica accumulation on beach morphodynamics: A remote sensing study. Coastal Engineering 205, 104933. https://doi.org/10.1016/j.coastaleng.2025.104933

Ticehurst, C., Karim, F., 2023. Towards developing comparable optical and SAR remote sensing inundation mapping with hydrodynamic modelling. International Journal of Remote Sensing 44 (9), 2912-2935. https://doi.org/10.1080/01431161.2023.2211714

Timmermans, B.W., Gommenginger, C.P., Dodet, G., Bidlot, J.R., 2020. Global Wave Height Trends and Variability from New Multimission Satellite Altimeter Products, Reanalyses, and Wave Buoys. Geophysical Research Letters 47 (9). https://doi.org/10.1029/2019gl086880

Tong, S.S., Deroin, J.P., Pham, T.L., 2020. An optimal waterline approach for studying tidal flat morphological changes using remote sensing data: A case of the northern coast of Vietnam. Estuarine, Coastal and Shelf Science 236, 106613. https://doi.org/10.1016/j.ecss.2020.106613

Tsai, Y.-L.S., 2022. Monitoring 23-year of shoreline changes of the Zengwun Estuary in Southern Taiwan using time-series Landsat data and edge detection techniques. Science of The Total Environment 839, 156310. https://doi.org/10.1016/j.scitotenv.2022.156310

Vitousek, S., Vos, K., Splinter, K.D., Erikson, L., Barnard, P.L., 2023. A Model Integrating Satellite-Derived Shoreline Observations for Predicting Fine-Scale Shoreline Response to Waves and Sea-Level Rise Across Large Coastal Regions. JGR Earth Surface 128 (7). https://doi.org/10.1029/2022jf006936

Vos, K., Harley, M.D., Splinter, K.D., Simmons, J.A., Turner, I.L., 2019. Sub-annual to multi-decadal shoreline variability from publicly available satellite imagery. Coastal Engineering 150, 160-174. https://doi.org/10.1016/j.coastaleng.2019.04.004

Wang, G., Mang, S., Cai, H., Liu, S., Zhang, Z., Wang, L., Innes, J.L., 2016. Integrated watershed management: evolution, development and emerging trends. J. For. Res. 27 (5), 967-994. https://doi.org/10.1007/s11676-016-0293-3

Wang, Y., Li, Y., Limaye, A.B., 2025. Bridging Gaps in Satellite Observations of River and Delta Landscapes Using Image Warping. Water Resources Research 61 (5). https://doi.org/10.1029/2024wr039854

Wu, B., Zhu, W., Yan, N., Xing, Q., Xu, J., Ma, Z., Wang, L., 2020. Regional Actual Evapotranspiration Estimation with Land and Meteorological Variables Derived from Multi-Source Satellite Data. Remote Sensing 12 (2), 332. https://doi.org/10.3390/rs12020332

Xiao, S., Xia, J., Zou, L., 2020. Evaluation of Multi-Satellite Precipitation Products and Their Ability in Capturing the Characteristics of Extreme Climate Events over the Yangtze River Basin, China. Water 12 (4), 1179. https://doi.org/10.3390/w12041179

Xie, H., Sun, Y., Liu, X., Xu, Q., Guo, Y., Liu, S., Xu, X., Liu, S., Tong, X., 2021. Shore Zone Classification from ICESat-2 Data over Saint Lawrence Island. Marine Geodesy 44 (5), 454-466. https://doi.org/10.1080/01490419.2021.1898498

Yan, N., Qiu, Z., Zhang, C., Liu, J., Liu, D., 2025. Observing water turbidity in Chinese rivers using Landsat series data over the past 40 years. Journal of Cleaner Production 494, 145001. https://doi.org/10.1016/j.jclepro.2025.145001

Yao, J., Xu, N., Wang, M., Liu, T., Lu, H., Cao, Y., Tang, X., Mo, F., Chang, H., Gong, H., Xin, H., Xu, H., 2025. SWOT satellite for global hydrological applications: accuracy assessment and insights into surface water dynamics. International Journal of Digital Earth 18 (1). https://doi.org/10.1080/17538947.2025.2472924

Young, I.R., Ribal, A., 2019. Multiplatform evaluation of global trends in wind speed and wave height. Science 364 (6440), 548-552. https://doi.org/10.1126/science.aav9527

Zagórski, P., Jarosz, K., Superson, J., 2020. Integrated Assessment of Shoreline Change along the Calypsostranda (Svalbard) from Remote Sensing, Field Survey and GIS. Marine Geodesy 43 (5), 433-471. https://doi.org/10.1080/01490419.2020.1715516

Zaitchik, B.F., Rodell, M., Reichle, R.H., 2008. Assimilation of GRACE Terrestrial Water Storage Data into a Land Surface Model: Results for the Mississippi River Basin. Journal of Hydrometeorology 9 (3), 535-548. https://doi.org/10.1175/2007jhm951.1

Zhao, Y., Fu, J.E., Pang, Z., Jiang, W., Zhang, P., Qi, Z., 2025. Validation of Inland Water Surface Elevation from SWOT Satellite Products: A Case Study in the Middle and Lower Reaches of the Yangtze River. Remote Sensing 17 (8), 1330. https://doi.org/10.3390/rs17081330

Zuniga-Teran, A.A., Fisher, L.A., Meixner, T., Le Tourneau, F.-M., Postillion, F., 2022. Stakeholder participation, indicators, assessment, and decision-making: applying adaptive management at the watershed scale. Environ Monit Assess 194 (3). https://doi.org/10.1007/s10661-021-09741-4